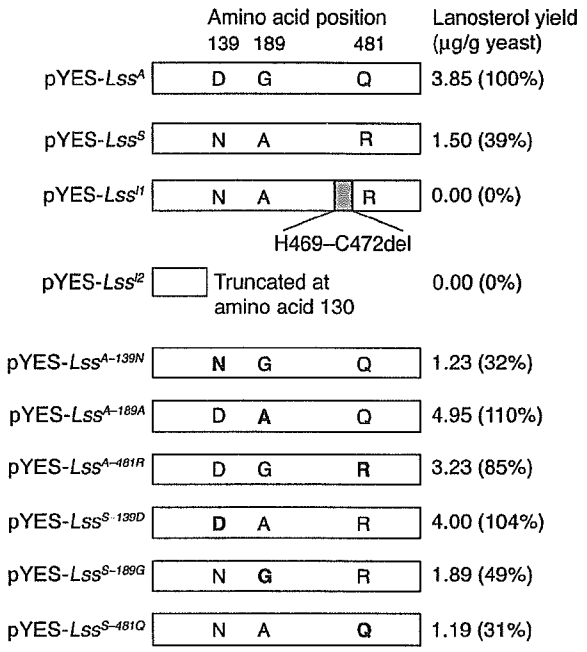

Figure 5
In vitro LSS activity measured as lanosterol yield in yeast. Amino acid variations of the isoforms expressed from each pYES construct are indicated by bold letters. The percentages in parentheses are calculated relative activity when the activity obtained from pYES-*Lss*^{A} was defined as 100%.

underlie this observation. Indeed, it has previously been postulated that a recessive cataract gene and a gene associated with embryonic lethality are required for cataract onset in SCRs (2). Taken together, our results strongly suggest that genes for cataract and embryonic lethality are alleles on the same *Cats1* locus, *Cats1*^{S} and *Cats1*^{I} (with S and I referring to SCR and lethal alleles, respectively). Therefore, the genotypes of cataractous and normal SCRs were assumed as *Cats1*^{S}/*Cats1*^{I} and *Cats1*^{S}/*Cats1*^{S}, respectively (Figure 1). Rats with the *Cats1*^{I}/*Cats1*^{I} genotype would die in utero. The ACI strain must carry a dominant *Cats1*^{A} allele. Accordingly, the (SCR × ACI)F_1 rats used for the production of F_2 progeny would have a *Cats1*^{A}/*Cats1*^{I} genotype, with the genotype of live-born (SCR × ACI)F_2 rats being either *Cats1*^{A}/*Cats1*^{A} or *Cats1*^{A}/*Cats1*^{I}, and all rats displaying a normal phenotype. The absence of cataracts in F_1 and F_2 rats with the *Cats1*^{A}/*Cats1*^{I} genotype would then be explained by assuming the order of dominance as follows: *Cats1*^{A}, *Cats1*^{S}, and *Cats1*^{I}.

Lss is a positional candidate for Cats1. If the above supposition is true, then the 4 F_2 rats with haplotypes 5–8 would be *Cats1*^{A}/*Cats1*^{I} heterozygotes. Therefore, we attempted to narrow down the region for *Cats1* by looking for loci where all 4 of the F_2 rats were heterozygous. The *Ggtp* locus is located near several genes including *Gnaz*, *Gstt2*, *S100b*, *Ftcd*, and *Lss* on mouse chromosome 10. Given syntenic conservation between rat chromosome 20 and mouse chromosome 10, we developed microsatellite markers within or close to the rat *Gnaz*, *Gstt2*, *S100b*, and *Ftcd* genes and genotyped the 4 F_2 rats for these markers. At least 1 of the rats was homozygous for SCR-derived alleles at these genes (Figure 2C), which meant none of these genes could be *Cats1*. For the remaining gene, *Lss*, we identified a single nucleotide polymorphism (SNP) in PCR products derived from ACI rats and SCRs (data not shown). All 4 rats were heterozygous for the *Lss* SNP, which suggested that *Lss* is in fact *Cats1* and that SCRs contain a genetic defect within the *Lss* locus. Also in support of this hypothesis is the fact that *Lss* codes for lanosterol synthase (also known as oxidosqualene cyclase; EC 5.4.99.7), which catalyzes the conversion of (3S)-2,3-oxidosqualene to lanosterol, and oral administration of LSS inhibitors is known to induce cataracts in rats (13–16), dogs, and mice (17).

The Lss gene is mutated in SCRs. We compared the nucleotide sequences of the Lss cDNA from ACI rats, cataractous SCRs, and normal SCR littermates. Two different cDNAs were obtained from normal SCRs (presumably with the *Lss*^{S}/*Lss*^{S} genotype). One sequence represented the same 2,202-bp open reading frame as the ACI-derived allele (*Lss*^{A}) except for 8 nucleotide substitutions, of which 5 were silent mutations (672C→T, 873T→C, 891G→A, 972T→C, and 993A→G). The remaining 3 nucleotide substitutions gave rise to missense mutations: 415G→A (D139N), 566G→C (G189A), and 1442A→G (Q481R) (Figure 3A). The other cDNA sequence from normal SCRs contained the same 8 substitutions as well as a 47-bp deletion (385–431del) that resulted in a reading frame shift and a protein truncated at amino acid position 130. This deletion was later found to be the result of alternative splicing from the *Lss*^{S} allele.

Four different cDNA sequences were obtained from cataractous SCRs (presumably having the *Lss*^{S}/*Lss*^{I} genotype). While 2 were identical to those obtained from normal SCRs (and therefore probably derived from the *Lss*^{S} allele), the third and fourth cDNA sequences contained a 13-bp deletion (1405–1417del) as well as a single nucleotide insertion (1419–1420insT) in the first and second types, respectively. The 1405–1417del plus the 1419–1420insT led to the loss of 4 amino acids in the LSS protein (H469–C472del) (Figure 3B). The third and fourth cDNA sequences were later found to be alternative splicing products from the *Lss*^{I} allele. Thus, 3 alleles (*Lss*^{A}, *Lss*^{S}, and *Lss*^{I}) were identified at the *Lss* locus, which was consistent with the presumption of 3 *Cats1* alleles and further supported the hypothesis that *Lss* and *Cats1* were the same locus.

Nucleotides 1405–1419 in Lss cDNA corresponded to positions 85 to 101 of exon 15 of the *Lss* gene. When we PCR amplified and sequenced *Lss* exon 15 from cataractous SCR, 2 different sequences were obtained: 1 with and 1 without the mutations corresponding to 1405–1417del and 1419–1420insT. Therefore, the 1405–1417del and 1419–1420insT alterations reflected genomic mutations.

Aberrant splicing of Lss mRNA is due to a single nucleotide substitution in exon 4. The 385–431del in Lss cDNA corresponded to the last 47 nucleotides (position 63 to 109) of exon 4 of the *Lss* gene. Examination of exon 4 sequences from normal and cataractous SCRs revealed that the 47 nucleotides missing from the mRNA

Table 1
Segregation at *D15Mor3* in (SCR × ACI) × SCR backcross rats with the *Lss*^{S}/*Lss*^{I} genotype

Genotype at	Phenotype		
D15Mor3	Cataractous	Normal	Total
S/S	52	0	52
S/A	28	22	50
Total	80	22	102

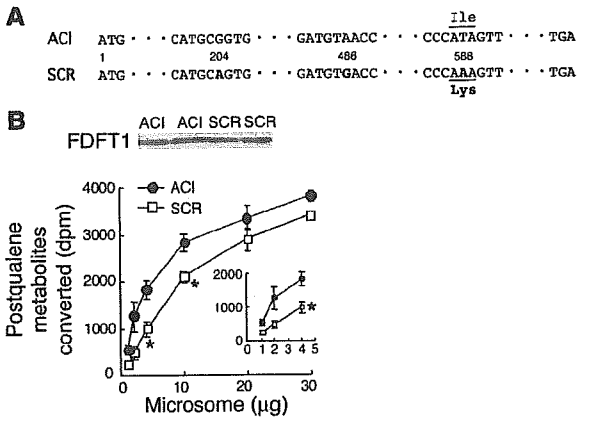

Figure 6

Fdft1 mutations and reduced FDFT1 activity in SCRs. (**A**) Alignment of regions of Fdft1 cDNA sequence derived from SCR and ACI rats. Nucleotide substitutions at positions 204, 486, and 588 in SCR *Fdft1* are indicated in bold. The I196K amino acid substitution caused by 588T→A is also shown. (**B**) Comparison of FDFT1 activity in rat liver microsome, as determined by amount of postsqualene metabolites converted from [^{3}H]farnesyl diphosphate (mean dpm ± SD). $^*P < 0.05$ versus ACI rats (Student's *t* test). Western blot image of rat hepatic FDFT1 is shown at the top.

were still present in genomic DNA. Indeed, only 1 difference was observed between the 2 *Lss* alleles, as position 93 in exon 4 contained a G in Lss^A but an A in Lss^S, which corresponds to the 415G→A substitution in Lss cDNA. Based on this finding, we hypothesized that the 385-431del in Lss cDNA was due to aberrant mRNA splicing that utilized the GpT at the 5′ end of 385-431del as a splice donor (Figure 4A). To confirm this hypothesis, chromosomal DNA spanning from exon 4 to exon 5 of both Lss^A and Lss^S alleles was transcribed in COS cells, and the resultant splicing pattern was examined. Only trace amounts of aberrant transcripts were observed for the Lss^A allele (Figure 4, B and C). On the other hand, aberrant transcripts were observed for the Lss^S allele, with the aberrant form accounting for about 40% of total transcripts, which was equivalent to that observed in SCR lenses and livers. These results suggest that the 385-431del in Lss cDNA was caused by aberrant splicing at position 72 in exon 4, and that the G→A substitution at position 93 in exon 4 was involved in this aberrant splicing. While the mechanisms for this shift in splice donor were unclear, it is possible that the substitution enhanced the affinity of the cryptic splicing site for the splicing apparatus, allowing it to compete with the intrinsic splice site. As an Lss^I minigene construct exhibited a splicing pattern similar to that of the Lss^S construct (data not shown), our results indicated that the 4 types of mRNA in cataractous SCRs represent normal and aberrant transcripts from Lss^S and Lss^I alleles.

Mutant LSS isoforms have reduced activity. We then measured LSS activity in the liver. The rate of conversion from oxidosqualene to lanosterol by liver microsomes of cataractous SCRs (Lss^S/Lss^I) was 42.9 ± 4.0 pmol/mg/min, which was significantly lower than the rate obtained from ACI rats (113.0 ± 11.1 pmol/mg/min; $P < 0.001$), but not different from that obtained from normal SCRs (Lss^S/Lss^S; 46.0 ± 4.5 pmol/mg/min). The finding that LSS activities were not different between cataractous and normal SCRs was puzzling. One hypothesis to account for this discrepancy is possible fluctuations in the proportion of aberrantly spliced mRNA. Indeed, we observed differences in the percentages of aberrantly spliced products (range, 31.5-78.8%; average, 40.5%) between rats, although deviations within individual rats were small (data not shown). The lack of difference in LSS activity between normal and cataractous SCRs might be explained if it is assumed that the percentage of aberrant transcripts was increased in normal SCRs or if the percentage of normal transcripts was increased in cataractous SCR used for the LSS activity assay.

To avoid this problem, each LSS isoform was expressed from cDNA in yeast, and LSS activity was assessed (Figure 5). Full-length LSS with the D139N, G189A, and Q481R amino acid substitutions (full-length form of the Lss^S allele) produced only about 39% of the lanosterol produced by full-length LSS encoded by the Lss^A allele. No lanosterol was produced from the H469-C472del Lss^I allele, and the LSS truncated at amino acid 130. These results clearly indicate that Lss^S and Lss^I are hypomorphic and null alleles, respectively. Furthermore, all 3 artificial isoforms carrying the D139N substitution showed reduced lanosterol production, which suggests that the D139N substitution was responsible for the diminished enzyme activity of Lss^S allele (Figure 5). Taken together, our results demonstrate that the G→A nucleotide substitution in exon 4 of the Lss^S allele leads to reduction of enzyme activity through the D139N amino acid substitution in addition to the activation of a cryptic splice donor.

$Cats2^A$ on chromosome 15 suppresses cataractogenesis. We genotyped the *Lss* locus of 80 cataractous backcross rats and confirmed that all rats were Lss^S/Lss^I heterozygotes. However, the frequency of cataractous rats was significantly lower than expected ratio of one-third (cataractous/normal, 80:225; $\chi^2 = 7.0$; $P < 0.01$). To determine whether some of the noncataractous rats carried the Lss^S/Lss^I heterozygous genotype, we genotyped all 225 normal backcross rats for the *Lss* locus and found that 22 rats were indeed Lss^S/Lss^I heterozygotes. Thus, the frequency of rats with the Lss^S/Lss^I genotype was not different from the expected one-third ($\chi^2 = 0.1$; $P > 0.1$). The absence of cataracts in these 22 Lss^S/Lss^I rats could be due to

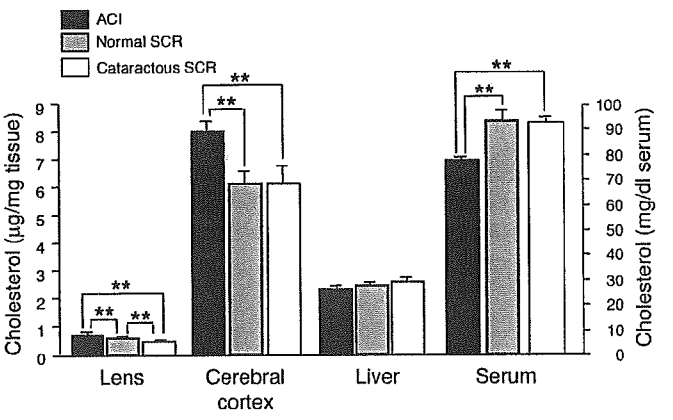

Figure 7

Comparison of tissue and serum cholesterol levels. The mean cholesterol content in ACI rats, normal SCR, and cataractous SCR ($n = 3$ per group) in the lens (0.74, 0.56, and 0.42 μg/mg wet tissue, respectively), frontal cerebral cortex (8.00, 6.15, and 6.15 μg/mg wet tissue, respectively), liver (2.24, 2.42, and 2.56 μg/mg wet tissue, respectively), and serum (77.3, 93.0, and 92.8 mg/dl, respectively) are shown. $^{**}P < 0.01$.

Table 2
Sterol profile in the rat lens

Rat strain	Squalene	2,3-oxidosqualene	Lanosterol	7-dehydrocholesterol	Desmosterol	Cholesterol
ACI	0.014 ± 0.010	0.005 ± 0.004	0.002 ± 0.001	0.005 ± 0.001	0.021 ± 0.008^A	0.740 ± 0.030^B
Normal SCR	0.019 ± 0.003	0.002 ± 0.001	0.001 ± 0.000^C	0.002 ± 0.000	0.032 ± 0.002^A	0.560 ± 0.010^B
Cataractous SCR	0.020 ± 0.001	0.002 ± 0.001	0.002 ± 0.000	0.001 ± 0.001	0.040 ± 0.001^A	0.423 ± 0.023^B

Values were calculated as μg/mg lens. $^A P < 0.05$, $^B P < 0.01$ between strains; $^C P < 0.05$ compared with ACI.

incomplete penetrance of the effect of the *Lss* mutation or to intervention by other gene(s) that prevent cataract onset. To investigate these possibilities, the 22 Lss^S/Lss^I rats without cataracts were genotyped for other marker loci. All 22 rats were heterozygous at the region between *D15Rat83* and *D15Rat97* (homozygosity/heterozygosity, 0:22; $\chi^2 = 22.0$; $P < 0.001$; Table 1). Meanwhile in cataractous rats, significant deviation toward homozygosity for SCR-derived alleles was observed at these loci (homozygosity/heterozygosity, 52:28; $\chi^2 = 7.2$; $P < 0.05$). Thus there appeared to be a gene on chromosome 15 of ACI rats that suppressed cataractogenesis (provisionally designated $Cats2^A$). The genetic effect of $Cats2^A$ appeared to be semidominant, as about 50% (22 of 50) of the rats with the $Cats2^S/Cats2^A$ genotype still developed cataracts. Haplotype analysis assigned the *Cats2* locus to the region between *D15Rat137* (9.57 cM) and *D15Rat102* (58.60 cM) (Figure 2D).

SCR has a mutation in the Fdft1 gene and reduced FDFT1 activity. The *Cats2* region seemed too large for positional cloning, but we examined 3 candidate genes for *Cats2*: *gap junction membrane channel protein, alpha 3* (*Gja3*); *Rab geranylgeranyl transferase, a subunit* (*Rabggta*); and *Fdft1*. These genes were selected because the null mutation of *Gja3* is known to lead to nuclear cataracts with crystallin proteolysis (18); RABGGTA shows protein prenylation activity, and the inhibition of prenylation of small GTP-binding proteins is an important factor in the lavastatin-induced rat cataract model (19); and FDFT1 (also known as squalene synthase; EC 2.5.1.21) functions 2 steps upstream of the LSS in the cholesterol biosynthesis pathway, catalyzing the condensation of 2 molecules of farnesyl pyrophosphate to form squalene. cDNA fragments covering the entire coding region of the 3 genes were PCR amplified from the lens mRNA of ACI rats and SCRs, run on an agarose gel, and sequenced. PCR products of *Gja3* and *Rabggta* mRNA derived from the SCR and ACI strains did not show apparent quantitative differences by agarose gel electrophoresis (data not shown). In addition, no strain-specific differences were identified in the cDNA sequences of either gene, which suggested that neither gene was *Cats2*.

Meanwhile, the sequence of Fdft1 cDNA revealed 3 nucleotide substitutions between ACI ($Fdft1^A$) and SCR ($Fdft1^S$). While 2 of these substitutions were silent (204G→A and 486A→G), the third substitution (588T→A) was a missense mutation, such that codon 196 was changed from ATA in ACI rats to AAA in SCRs, which resulted in an I196K substitution (Figure 6A). Western blot analysis indicated that roughly equal amounts of FDFT1 were expressed in the livers of SCR and ACI rats (Figure 6B). However, FDFT1 activity in liver microsomal fractions was significantly lower in SCR than in ACI rats, which indicated that the $Fdft1^S$ was a hypomorphic allele. The relatively slight increase in FDFT1 activity in ACI rats appeared to agree well with the semidominant effect of the $Cats2^A$ locus. While the results presented in this report are admittedly not sufficient to substantiate the hypothesis that mutated *Fdft1* is $Cats2^S$, we believe that the *Fdft1* is a strong candidate for the *Cats2*, because in particular FDFT1 functions 2 steps upstream of LSS in the cholesterol biosynthesis pathway. It is at least conceivable that cholesterol biosynthesis was further disturbed by the mutant *Fdft1* in SCR, thereby rendering the rats more susceptible to cataracts, and $Fdft1^A$ allele suppressed cataractogenesis by more efficiently catalyzing squalene production.

The SCR lens has low cholesterol content. We then examined lens cholesterol content. Lenses of normal SCRs (Lss^S/Lss^S) and cataractous SCRs (Lss^S/Lss^I) had cholesterol contents that were 76%

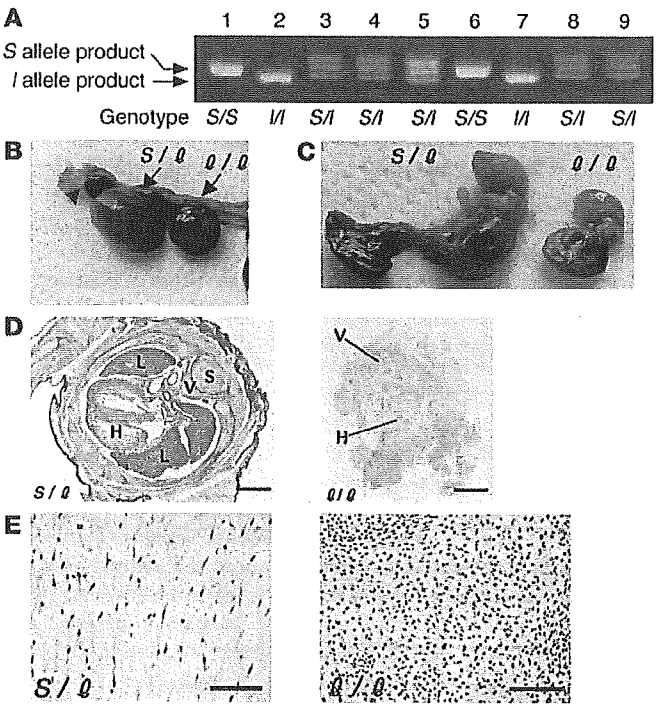

Figure 8
Phenotype of Lss^I/Lss^I embryos. (**A**) Agarose gel electrophoresis image of the genotype analysis for a litter of E12.5 embryos. (**B**) Gross appearance of part of a uterus with embryos at E16.5. Two embryos covered with the yolk sac are indicated by arrows. One embryo (arrowhead) shows resorption, leaving only placenta. (**C**) Gross appearance of normal (left) and Lss^I/Lss^I embryos (right) shown in **B**, taken out of the yolk sac with the placenta. (**D**) Cross sections of the same embryos shown in **C**. H, heart; V, vertebra; S, spinal cord; L, lung. (**E**) Higher magnification of mesenchymal tissues. Scale bars: 1 mm (**D**); 100 μm (**E**).

Table 3
Frequency of genotypes in offspring from intercross of Lss^S/Lss^I rats

Age	No. litters	Lss^S/Lss^S	Lss^S/Lss^I	Lss^I/Lss^I	Resorbed	Total
E9.5	2	3	9	4	0	16
E12.5	3	7	15	5	0	27
E14.5	4	6	14	2	8	30
E16.5	3	10	12	3	5	30
E18.5	3	8	13	0	7	28
Postnatal	2	4	10	0	NA	14

and 57% that of ACI lenses, respectively (Figure 7). Similar levels of oxidosqualene and lanosterol were observed in all 3 rat groups (Table 2). This finding appeared to be inconsistent with the expectation that cataractous lenses would contain more oxidosqualene and less lanosterol due to the deficient conversion of oxidosqualene to lanosterol in SCRs. However, this discrepancy may be explained by the swift turnover of sterol intermediates to cholesterol. Consistent with this, 5 sterol intermediates measured in this study accounted for only approximately 2–5% of lens cholesterol (Table 2). Several small peaks indicative of the presence of other intermediates were also observed in a gas-liquid chromatography analysis (data not shown). These peaks also accounted for a small percentage cholesterol and did not show a difference among the 3 rat groups. Thus it was unlikely that oxidosqualene was converted to an unusual compound that could be toxic and accumulate in cataractous lenses. Exceptionally, desmosterol contents were significantly higher in cataractous lenses than in normal lenses, yet the absolute quantities were minute. The cause of this desmosterol accumulation, as well as its association with LSS deficiency, is unclear. The conversion of 7-dehydrodesmosterol to desmosterol occurs downstream of the LSS step in the cholesterol biosynthesis pathway, such that the accumulation of desmosterol cannot be explained by LSS deficiency. Taken together, our data suggest that cataracts in SCRs are the result of reduced cholesterol in the lenses rather than the accumulation of sterol intermediates in the pathway prior to lanosterol synthase.

Phenotypic characterization of Lss^I/Lss^I homozygous embryos. The fact that Lss^I is a null allele may well explain the lethality of Lss^I/Lss^I homozygous embryos. To determine at which developmental stage lethality occurred in affected embryos, embryos at different embryonic stages were harvested and genotyped. At E12.5, embryos with the Lss^S/Lss^S, Lss^S/Lss^I, and Lss^I/Lss^I genotypes were identified at the expected Mendelian frequency of 1:2:1 (Figure 8A and Table 3). However, the Lss^I/Lss^I embryos already appeared to be smaller than Lss^S/Lss^I and Lss^S/Lss^S littermates. At E14.5, a significant number of embryos had exhibited resorption, which left only a trace of embryo within a well-developed placenta (Figure 8B). Genotyping of these embryos was impossible, as DNA could not be recovered. However, of the remaining embryos, the frequency of the Lss^I/Lss^I genotype was significantly lower than expected, which suggested that the resorbed embryos were Lss^I/Lss^I. The remaining Lss^I/Lss^I embryos appeared severely growth retarded. The requirement of cholesterol for cell growth and division of mammalian cells has been previously reported (20–22). In rodents, maternal cholesterol can cross the placenta and appears to be essential for early fetal development (23), but ceases to be effective beyond midgestation when a functional cholioallantoic circulatory system is established (24). The timing of SCR embryo death appeared to correspond with this period. Nonetheless, a few retarded Lss^I/Lss^I embryos could still be recovered beyond E16.5 (Figure 8C). The major pathological abnormality in these embryos was defective organogenesis (Figure 8D), with skin and nerve tissues, as well as major internal organs, hardly discernible. The anatomical location of organs was also disturbed. Lss^I/Lss^I embryos also displayed abnormal mesenchymal tissues (Figure 8E). These mesenchymal cells were small and oval shaped with large nuclei and high cellularity, which was suggestive of immature status. At E18.5, no Lss^I/Lss^I embryos were identified. Thus, it appeared that the major cause of prenatal death of Lss^I/Lss^I embryos was dysorganogenesis due to poor cellular proliferation.

Discussion

Our data identified mutations in the gene for LSS, part of the cholesterol biosynthesis pathway, as the underlying cause of cataracts in the SCR strain and indicated that the SCR represents a new example of hereditary cholesterol deficiency–associated cataracts. Our findings may have implications for 2 known clinical settings: patients with malformation syndromes due to inborn defects of cholesterol synthesis and individuals taking cholesterol-lowering medication. To date, 6 inborn defects of cholesterol biosynthesis have been described in humans (reviewed in refs. 25, 26), and 3 of the associated conditions have cataracts as complications: mevalonic aciduria (27–29), Smith-Lemli-Opitz syndrome (30–32), and X-linked dominant chondroplasia punctata 2 (33, 34). The cause of cataracts in these diseases was postulated to be due to the decrease in cholesterol level in the lens. Alternatively, the cataracts may reflect a response to the accumulation of precursors in the cholesterol biosynthesis pathway. Our data showing reduced cholesterol level without accumulation of sterol precursors in the SCR lens supports the hypothesis that the common cause of cataracts in these diseases is in fact cholesterol deficiency. Thus the cataracts in these conditions may share developmental features with the SCR model.

The continuous appearance of poorly differentiated epithelial cells at the bow area of the lens is thought to be the pathophysiological basis for cataract formation in the SCR (3). It is thought that the lens derives its cholesterol from de novo synthesis in situ, as vertebrate eye lenses are nonvascularized (35). The vertebrate eye lens contains only a single layer of epithelial cells on its anterior surface. The epithelial cells remain quiescent in the central section of the lens surface, divide toward the equatorial area, and terminally differentiate into fiber cells in the equatorial regions. Cholesterol is required for membrane formation by these proliferating lens epithelial cells to proceed through cell cycle (36). The importance of the epithelial cells is further inferred from the fact that mature lens fiber cells lose their nuclei and other cytosolic organelles during differentiation, and with them the ability to synthesize cholesterol. For these reasons, the lens may be especially vulnerable to the effect of low cholesterol. Based on these observations, we postulated a mechanism for cataract development in SCRs whereby SCR lens epithelial cells unable to synthesize sufficient cholesterol for proper proliferation caused the loss of homeostatic epithelial cell control of the underlying fiber cells, leading to the sequence of biochemical abnormalities observed in

the SCR, from increased cellular calcium (9) to calpain activation (10, 11), enhancement of proteolysis of crystallins and cytoskeletal proteins (12), and eventually protein insolubilization that is responsible for lens opacification.

Intriguingly, it has been pointed out that lens epithelial cell apoptosis could be a common initial cause of noncongenital cataracts (5–8). A typical lens undergoes a series of changes during the cataractous process. First, separation and liquefaction of the anterior suture occur, after which the separated part of the anterior suture gradually becomes covered by proliferative epithelial cells. As a consequence, lens fiber cells regenerate, leading to the recovery of lens transparency. However, upon the completion of repair these proliferative epithelial cells gradually decrease in number and become vacuolated and swollen with age, such that recovery of the cataract is halted. This process shows the importance of the differentiating and metabolizing functions of the epithelial cells in lens reconstruction and raises the possibility that transplantation of normal lens epithelial cells could prevent and/or recover the cataractous lens in SCRs as well as assist in the development of a novel therapeutic and/or prophylactic approaches to human cataracts.

Other abnormal phenotypes observed in human patients with hereditary defects in the cholesterol biosynthesis pathway, such as dysmorphic development, mental retardation, and behavioral phenotype due to neurological defects, are not apparent in SCRs. Compared with ACI rats, the cholesterol content of the frontal cerebral cortex of both normal (Lss^S/Lss^S) and cataractous SCRs (Lss^S/Lss^I) was reduced by 24% (Figure 7), which still might be sufficient for normal brain development and function. In the liver, LSS activity in SCRs was only about 40% that of the ACI rats. However, as there were no discernible liver abnormalities in SCR, it appears that the reduced LSS activity was still enough to maintain liver cholesterol levels.

Interfering with cholesterol biosynthesis using drugs is an effective therapeutic approach to lower elevated plasma cholesterol levels and the risks of coronary heart disease. Although these drugs are relatively safe, there are still concerns regarding toxicity. Whether cataract occurrence is increased in patients treated with cholesterol-lowering medications remains uncertain. Of the cholesterol-lowering agents currently used, statins, which function as potent inhibitors of hydroxymethyl glutaryl coenzyme A (HMG-CoA) reductase, are the most prescribed group of drugs. While results of clinical safety trials collectively show no higher risk of cataracts in statin-treated patients (26), Schlienger et al. (37) reported that concomitant use of erythromycin and simvastatin might increase cataract risk in humans. Erythromycin is thought to block statin metabolism by the cytochrome P-450 system, thereby increasing the serum levels of statins and the risk for toxicity.

Meanwhile, it has been demonstrated in toxicity tests using animals that several drugs that inhibit lens cholesterol biosynthesis can produce cataracts (reviewed in ref. 26). For instance, vastatin causes cataracts in dogs (38). Another group of agents, lanosterol synthase inhibitors, induce cataracts in rats (13–16), mice, and dogs (17). Above all, the cataracts caused by 3-β(2-diethylaminoethoxy)-androst-5-en-17-one hydrochloride (U18666A) have been intensively studied. Results from the U18666A-induced rat cataract model suggested that total lens cholesterol content needed to be decreased by 30–70% for cataract onset (13–16). More recent reports suggest that the cataractogenic effect of U18666A might be related to direct perturbation of lens membrane structure and function (39). In the SCR model, cataracts occurred only in rats heterozygous for the hypomorphic Lss^S and null Lss^I alleles, but not in those homozygotes for the Lss^S allele. Lenses of cataractous SCRs (Lss^S/Lss^I) and normal SCRs (Lss^S/Lss^S) had cholesterol contents that were 57% and 76% that of ACI lenses, respectively. These results support the hypothesis that cholesterol deficiency alone may induce cataracts, even though the possibility of direct perturbation by U18666A cannot be excluded. Our data also underpinned the hypothesis that there was a distinctive threshold between 57% and 76% for lens cholesterol level in cholesterol deficiency–associated cataracts. Threshold cholesterol levels for other organs to maintain normality could not be defined in the SCR model. Defining the threshold should be particularly important, considering that there is no known cure for human syndromes resulting from impaired cholesterol biosynthesis and that cholesterol supplementation is proposed as 1 possible therapy.

Our data also underscored the possibility that even a slight change at a single step in the cholesterol biosynthesis pathway (FDFT1 in the case of the SCR) could compound susceptibility to cholesterol deficiency–associated cataracts when another step (LSS in the case of the SCR) is also restrained. Intriguingly, simvastatin is cataractogenic when administered orally to a specific strain of Wistar rats (40). It was postulated that this rat strain carried a genetic defect in the regulation of a key enzyme downstream of mevalonic acid in the cholesterol biosynthesis pathway that rendered the rats more susceptible to the cataractogenic effects of simvastatin. It is possible that hypomorphic genetic polymorphisms exist in cholesterol biosynthesis genes in humans similar to those seen in rats. The presence of such polymorphisms has been inferred from the observations in Smith-Lemli-Opitz syndrome. These patients have the mutations in the gene for *3β-hydroxysterol Δ⁷-reductase* (*DHCR7*), and hence have defects in cholesterol biosynthesis. However, there is a remarkable difference in phenotypic severity even between patients with identical *DHCR7* mutations. Thus, it has been postulated that other genetic as well as developmental or maternal factors perhaps affecting cholesterol biosynthesis or homeostasis significantly influence a given patient's phenotype. If in fact hypomorphic genetic polymorphisms exist in cholesterol biosynthesis genes in humans, then it is possible that such people would be at a higher risk for cataracts when receiving statins or other cholesterol-lowering agents. Conversely, exploration of these polymorphisms may shed a new light on the clinical studies of disorders such as Smith-Lemli-Opitz syndrome.

In conclusion, we have identified the molecular genetic basis of cataract onset in the SCR strain. The SCR model represents what we believe to be a new example of hereditary cholesterol deficiency–associated cataracts and should prove useful in the development of therapeutic and/or preventive measures for cataracts.

Methods

Genetic linkage analysis of cataracts. Normal SCRs, cataractous SCRs, and ACI rats were maintained at the Department of Laboratory Animal Science of the Tokyo Metropolitan Institute of Gerontology. Protocols used in this study were approved by the institute's review board. Cataractous SCRs (putative genotype, $Cats1^S/Cats1^I$) were crossed to ACI rats ($Cats1^A/Cats1^A$) to give (SCR × ACI)F_1 rats (Figure 1). To distinguish F_1 rats with and without $Cats1^I$, a prerequisite for cataract onset, rats were crossed with normal SCRs ($Cats1^S/Cats1^S$). F_1 rats that had cataractous progeny were judged as having the $Cats1^I$ allele ($Cats1^A/Cats1^I$). These F_1 rats were intercrossed or crossed with cataractous SCRs to give (SCR × ACI)F_2 and (SCR × ACI) × SCR

backcross rats. Rats were diagnosed for cataracts at 12 weeks of age by visual inspection and then sacrificed, and liver genomic DNA was extracted. Rats were genotyped for 78 microsatellite marker loci dispersed throughout the genome, and genetic linkage of the markers with cataracts was evaluated by the χ^2 test with a P value smaller than 0.05 being accepted as evidence of linkage.

Positional cloning of the cataract gene. Five genes (*Gnaz*, *Gstt2*, *S100b*, *Lss*, and *Ftcd*) located centromeric or telomeric to the *Ggtp* locus were selected from the mouse supercontig data. Rat contigs containing these genes were obtained by BLAST search using the mouse cDNA sequences against the NCBI rat contig databank (http://www.ncbi.nlm.nih.gov/genome/seq/RnBlast.html). Microsatellites identified in the contigs were examined for polymorphisms between SCRs and ACI rats, with the polymorphic microsatellites then used for the linkage study. Oligonucleotide primers for rat Lss cDNA were designed based on the reported sequence (U31352). Nucleotide sequences of the primers were as follows: Lss-1, 5′-GTGGTCCAGAGCTGTGCTGT-3′; Lss-2, 5′-TGGACTTGTCCTCAATGTGC-3′; Lss-19, 5′-GTCTCCTGATTACGTGTCACATAGC-3′; Lss-4, 5′-TTGATCCTCGAGACGTGCTC-3′; Lss-5, 5′-ATTCGTTGGTCAGTGGACGG-3′; Lss-6, 5′-TTGATCCTCGAGACGTGCTC-3′; Lss-7, 5′-ACAGGGCTACAGAGATCAGG-3′; Lss-8, 5′-GGACGCTTATCACCCAGCTG-3′; Lss-11, 5′-CTTCAGCACACTGGACTGT-3′; Lss-12, 5′-GGCTTTAGACTGATGTCCTAC-3′. Lens mRNA was extracted from SCRs and ACI rats using the QuickPrep Micro mRNA Purification Kit (Amersham Biosciences). First-strand cDNA was synthesized using a First-Strand cDNA Synthesis Kit (Amersham Biosciences), and cDNA fragments containing the entire *Lss* coding sequence were PCR amplified. An aliquot of each PCR product was then subjected to agarose gel electrophoresis. PCR products were directly sequenced using the primers used for PCR amplification or cloned into the pCR2.1 plasmid vector (Invitrogen Corp.).

LSS activity assay. The LSS activity assay for liver microsomal fractions was performed as previously described (41). Yeast expression constructs were made by cloning cDNA fragments for the 4 LSS isoforms into the pYES2.1 plasmid (Invitrogen Corp.), resulting in pYES-Lss^A, pYES-Lss^S, pYES-Lss^H, and pYES-Lss^{I2} (Figure 5). Nucleotide substitutions were introduced into the pYES-Lss^A and pYES-Lss^S using the GeneEditor In Vitro Site-Directed Mutagenesis System (Promega), resulting in pYES-$Lss^{A\ 139N}$, pYES-$Lss^{A\ 189A}$, pYES-$Lss^{A\ 481R}$, pYES-$Lss^{S\ 139D}$, pYES-$Lss^{S\ 189G}$, and pYES-$Lss^{S\ 481Q}$. The LSS-deficient yeast strain, SGL9, was transformed with the constructs, and LSS expression was induced as previously described (42). LSS activity was assessed as the conversion rate from [^{3}H]2,3-oxidosqualene to lanosterol (42). Three separate assays were performed for each construct.

Aberrant splicing of Lss exon 4. Chromosomal DNA sequence from exon 4 to exon 5 of the *Lss* gene was PCR amplified from genomic DNA from normal SCRs, cataractous SCRs, and ACI rats using the Lss-19/Lss-2 primer pair (Figure 4C). PCR products were subcloned into the pEF6/V5-His-TOPO plasmid (Invitrogen Corp.), resulting in pEF-Lss^A–exon4/5 and pEF-Lss^S–exon4/5. These minigene constructs were introduced into COS cells using Effectene Transfection Reagent (QIAGEN), and mRNA was isolated from the cells 2 days after transfection. This mRNA was reverse transcribed and PCR amplified using primers Lss-2 and Lss-19 that was 5′ end-labeled with HEX dye. PCR consisted of 18–32 cycles to give logarithmic phase amplification. The PCR products were run on an ABI PRISM 310 Genetic Analyzer (Applied Biosystems), and aberrant and normally spliced products were quantified by the GeneScan Analysis Software (version 2.1.1; Applied Biosystems).

FDFT1 activity assay. Rabbit polyclonal antibody was raised against FDFT1 protein expressed in *E. coli* and purified following previously described procedures (43) with minor modifications. Aliquot of 10 μg liver microsomal protein were separated by SDS-polyacrylamide gel electrophoresis and transferred onto PVDF membranes. Membranes were then reacted with the antiserum and detected with ImmunoStar Reagents (Wako Pure Chemical Industries Ltd.) for chemical luminescence. Signal densities on X-ray films were determined using an ATTO densitograph 4.1 system (ATTO). The FDFT1 activity assay was performed on liver microsomal fractions basically as previously described (44).

Sterol measurement. Three rats were used per group. Blood samples were collected after overnight fasting, and ocular lenses and part of the liver and frontal cerebral cortex were removed and homogenized in distilled water. Total lipids were extracted by the standard Bligh-Dyer method. Total cholesterol content was measured by enzymatic methods (Determiner TC555; Kyowa Medex Co. Ltd.), and difference in mean cholesterol content was evaluated by 2-tailed Student's t test. For determination of sterol profile, squalene, 2,3-oxidosqualene, lanosterol, 7-dehydrocholesterol, and desmosterol were purchased from Sigma-Aldrich and used as standards in a gas-liquid chromatography using a GC-17A gas chromatograph (Shimadzu Corp.) equipped with a chemically bonded fused silica SPB-1 capillary column (Sigma-Aldrich). Two lenses from each rat were combined, and 100 μg 5α-cholestane was added as an internal calibration standard. Sterols were extracted with chloroform-methanol and quantified by gas-liquid chromatography.

Examination of embryos. Embryos were harvested from timed matings of cataractous SCR. Genotyping of embryos and adult rats was performed on DNA isolated from embryo samples or adult tail tips by PCR amplification using an Lss-11 and Lss-12 primer pair (Figure 3A) that could differentiate the presence (Lss^S allele) and absence (Lss^I allele) of a 13-bp sequence (Figure 8A). PCR products were run on 4% NuSieve agarose gel. Embryos were fixed using buffered formalin, embedded in paraffin, and stained with hematoxylin and eosin.

Acknowledgments

This work was supported in part by a Grant-in-Aid for Scientific Research from the Japan Society for the Promotion of Science (17500286).

Received for publication December 12, 2003, and accepted in revised form November 22, 2005.

Address correspondence to: Masayuki Mori, Department of Aging Biology, Institute on Aging and Adaptation, Shinshu University Graduate School of Medicine, 3-1-1 Asahi, Matsumoto 390-8621, Japan. Phone: 81-263-37-2692; Fax: 81-263-37-3428; E-mail: masamori@sch.md.shinshu-u.ac.jp.

1. Tripathi, B.J., Tripathi, R.C., Borisuth, N.S., Dhaliwal, R., and Dhaliwal, D. 1991. Rodent models of congenital and hereditary cataract in man. *Lens Eye Toxic. Res.* **8**:373–413.
2. Shumiya, S. 1995. Esrablishment of rhe hereditary cararact rat strains (SCR) and genetic analysis. *Lab. Anim. Sci.* **45**:671–673.
3. Okano, T., Uga, S., Ishikawa, S., and Shumiya, S. 1993. Histopathological study of hereditary cataractous lenses in SCR strain rat. *Exp. Eye Res.* **57**:567–576.
4. Okano, T., Uga, S., Ishikawa, S., Hara, A., and Shumiya, S. 1999. Lens reconstruction after cataract in SCR rat. *Jpn. J. Opthalmol.* **43**:363–367.
5. Hightower, K.R., and McCready, J.P. 1991. Effect of selenite on epithelium of cultured rabbit lens. *Invest. Ophthalmol. Vis. Sci.* **32**:406–409.
6. Li, W.C., and Spector, A. 1996. Lens epithelial cell apoptosis is an early event in the development of UVB-induced cataract. *Free Radic. Biol. Med.* **20**:301–311.
7. Takamura, Y., Kubo, E., Tsuzuki, S., and Akagi, Y. 2003. Apoptotic cell death in the lens epithelium of rat sugar cataract. *Exp. Eye Res.* **77**:51–57.
8. Li, W.C., et al. 1995. Lens epithelial cell apoptosis appears to be a common cellular basis for non-congenital cataract development in humans and animals. *J. Cell Biol.* **130**:169–181.
9. Inomata, M., Hayashi, M., Shumiya, S., Kawashima, S., and Ito, Y. 2001. Involvement of inducible nitric oxide synthase in cataract formation in Shumiya cataract rats (SCR). *Curr. Eye Res.* **23**:307–311.
10. Inomata, M., et al. 1997. Evidence for the involve-

ment of calpain in cataractogenesis in Shumiya cataract rat (SCR). *Biochim. Biophys. Acta.* **1362**:11–23.
11. Inomata, M., Hayashi, M., Shumiya, S., Kawashima, S., and Ito, Y. 2000. Aminoguanidine-treatment results in the inhibition of lens opacification and calpain-mediated proteolysis in Shumiya cataract rats (SCR). *J. Biochem.* **128**:771–776.
12. Zhang, H., et al. 2001. Peptidases play an important role in cataractogenesis: an immunohistochemical study on lenses derived from Shumiya cataract rats. *Histochem. J.* **33**:511–521.
13. Cenedella, R.J., and Bierkamper, G.G. 1979. Mechanism of cataract production by 3-beta(2-diethyl aminoethoxy)andost-5-en-17-one hydrochloride, U18666A: an inhibitor of cholesterol biosynthesis. *Exp. Eye Res.* **28**:673–688.
14. Cenedella, R.J. 1983. Source of cholesterol for the ocular lens, studied with U18666A: a cataract-producing inhibitor of lipid metabolism. *Exp. Eye Res.* **37**:33–43.
15. Cenedella, R.J. 1985. Regional distribution of lipids and phospholipase A2 activity in normal and cataractous rat lens. *Curr. Eye Res.* **4**:113–120.
16. Yadav, S., and Rawal, U.M. 1992. Cholesterol and lipid peroxidation in 3beta-(2-diethylaminoethoxy)-androst-5-en-17-oneHCl (U18666A) induced cataractogenesis in rats. *Indian J. Exp. Biol.* **30**:147–148.
17. Pyrah, I.T., et al. 2001. Toxicologic lesions associated with two related inhibitors of oxidosqualene cyclase in the dog and mouse. *Toxicol. Pathol.* **29**:174–179.
18. Gong, X., et al. 1997. Disruption of alpha3 connexin gene leads to proteolysis and cataractogenesis in mice. *Cell.* **91**:833–843.
19. Cheng, Q., Robinson, W.G., and Zigler, J.S., Jr. 2002. Geranylgeranyl pyrophosphate counteracts the cataractogenic effect of lovastatin on cultured rat lenses. *Exp. Eye Res.* **75**:603–609.
20. Chen, H.W., Heininger, H.J., and Kandutsch, A.A. 1975. Relationship berween sterol synthesis and DNA synthesis in phytohemagglutinin-stimulated mouse lymphocytes. *Proc. Natl. Acad. Sci. U. S. A.* **72**:1950–1954.
21. Martinez-Botas, J., et al. 2001. Dose-dependent effects of lovastatin on cell cycle progression. Distinct requirement of cholesterol and non-sterol mevalonate derivatives. *Biochim. Biophys. Acta.* **1532**:185–194.
22. Suarez, Y., et al. 2005. Sterol stringency of proliferation and cell cycle progression in human cells. *Biochim. Biophys. Acta.* **1734**:203–213.
23. Dietschy, J.M., and Turley, S.D. 2002. Control of cholesterol turnover in the mouse. *J. Biol. Chem.* **277**:3801–3804.
24. Jollie, W.P. 1990. Development, morphology, and function of the yolk-sac placenta of laboratory rodents. *Teratology.* **41**:361–381.
25. Porter, F.D. 2002. Malformation syndromes due to inborn errors of cholesterol synthesis. *J. Clin. Invest.* **110**:715–724. doi:10.1172/JCI200216386.
26. Cendella, R.J. 1996. Cholesterol and cataracts. *Surv. Ophthalmol.* **40**:320–337.
27. Berger, S., Smit, G.P., Schierbeek, H., Bijsterverd, K., and le Coultre, R. 1985. Mevalonic aciduria: an inborn error of cholesterol biosynthesis? *Clin. Chim. Acta.* **152**:219–222.
28. Hoffman, G., et al. 1986. Mevalonic aciduria-an inborn error of cholesterol and nonsterol isoprene biosynthesis. *N. Engl. J. Med.* **314**:1610–1614.
29. Hoffman, G.F., et al. 1993. Clinical and biochemical phenotype in 11 patients with mevalonic aciduria. *Pediatrics.* **91**:915–921.
30. Cotlier, E., and Rice, P. 1971. Cataracts in the Smith-Lemli-Opitz syndrome. *Am. J. Ophthalmol.* **72**:955–959.
31. Gold, J.D., and Pfaffenbach, D.D. 1975. Ocular abnormalities in the Smith-Lemli-Opitz syndrome. *J. Pediatr. Ophthalmol.* **12**:228–234.
32. Kretzer, F.L., Hittner, H.M., and Mehta, R.S. 1981. Ocular manifestations of the Smith-Lemli-Opitz syndrome. *Arch. Ophthalmol.* **99**:2000–2006.
33. Happle, R. 1979. X-linked dominant chondrodysplasia punctata. Review of literature and report of a case. *Hum. Genet.* **53**:65–73.
34. Happle, R. 1995. X-linked dominant chondrodysplasia punctata/ichthyosis/cataract syndrome in males [letter]. *Am. J. Med. Genet.* **57**:493.
35. Cenedella, R.J. 1982. Sterol synthesis by the ocular lens of the rat during postnatal development. *J. Lipid Res.* **23**:619–626.
36. El-Sayed, G.N., and Cenedella, R.J. 1987. Relationship of cholesterolgenesis to DNA synthesis and proliferation by lens epithelial cells in culture. *Exp. Eye Res.* **45**:443–451.
37. Schlienger, R.G., Haefeli, W.E., Jick, H., and Meier, C.R. 2001. Risk of cataracts in patients treated with statins. *Arch. Intern. Med.* **161**:2021–2026.
38. Gerson, R.J., et al. 1990. On the etiology of subcapsular lericular opacities produced in dogs receiving HMG-CoA reducrase inhibitors. *Exp. Eye Res.* **50**:65–78.
39. Cenedella, R.J., et al. 2004. Direct perturbation of lens membrane structure may contribute to cataracts caused by U18666A, an oxidosqualene cyclase inhibitor. *J. Lipid Res.* **45**:1232–1241.
40. Cenedella, R.J., Kuszak, J.R., Al-Ghoul, K.J., Qin, S., and Sexton, P.S. 2003. Discordant expression of the sterol pathway in lens underlies simvastatin-induced cataracts in Chbb:Thom rats. *J. Lipid Res.* **44**:198–211.
41. Abe, I., Bai, M., Xiao, X., and Prestwich, G.D. 1992. Affinity labeling of vertebrate oxidosqualene cyclases with a tritiated suicide substrate. *Biochem. Biophys. Res. Commun.* **17**:32–38.
42. Abe, I., and Prestwich, G.D. 1995. Molecular cloning, characterization, and funcrional expression of rat oxidosqualene cyclase cDNA. *Proc. Natl. Acad. Sci. U. S. A.* **92**:9274–9278.
43. Thompson, J.F., et al. 1998. Truncation of human squalene synthase yields active, crystallizable protein. *Arch. Biochem. Biophys.* **350**:283–290.
44. Ishihara, T., Kakuta, H., Moritani, H., Ugawa, T., and Yanagisawa, I. 2004. Synthesis and biological evaluation of novel propylamine derivatives as orally active squalene synthase inhibitors. *Bioorg. Med. Chem.* **12**:5899–5908.

American Journal of Gastroenterology
© 2005 by Am. Coll. of Gastroenterology
Published by Blackwell Publishing

ISSN 0002-9270
doi: 10.1111/j.1572-0241.2005.00265.x

Expression of Fas Ligand by Hepatic Macrophages in Patients with Fulminant Hepatic Failure

Atsuyoshi Mita, M.D.,[1] Yasuhiko Hashikura, M.D.,[1] Yoh-ichi Tagawa, Ph.D.,[2] Jun Nakayama, M.D.,[3] Masatomo Kawakubo, Ph.D.,[3] and Shin-ichi Miyagawa, M.D.[1]

[1]*Department of Surgery, Shinshu University School of Medicine,* [2]*Department of Organ Regeneration, Shinshu University Graduate School of Medicine, and* [3]*Department of Pathology, Shinshu University School of Medicine, Matsumoto, Japan*

OBJECTIVES: The mechanisms of Fas–Fas ligand (Fas–FasL)-mediated apoptosis in the pathogenesis of fulminant hepatic failure (FHF) have not been well defined. This clinical study was carried out to assess which cells expressed Fas–FasL and to determine their involvement.

METHODS: The subjects were 24 patients with FHF who underwent liver transplantation at our institution. For comparison, nine chronic hepatitis (CH) patients and six living liver donors (LD) were also enrolled. Liver tissues were obtained for histological (hematoxylin–eosin, terminal deoxynucleotidyl transferase [TdT]-mediated dUTP-biotin nick-end labeling [TUNEL], immunohistochemistry, and double immunofluorescence staining) and reverse transcription PCR (RT-PCR; cytokines and chemokines) analysis.

RESULTS: The numbers of TUNEL-, FasL-, and CD68-positive cells in the livers of patients with FHF were significantly larger than in those with CH or with normal livers. Double immunofluorescence staining showed that FasL was expressed predominantly on liver macrophages and rarely on CD8-positive lymphocytes. RT-PCR study showed increased expression of FasL; interferon-γ; interleukin-18; macrophage inhibitory protein-1β; and regulated upon activation, normal T cell expressed and secreted in the livers of patients with FHF compared with those of LD.

CONCLUSIONS: Macrophages and their expression of FasL may play roles in the pathogenesis of FHF.

(Am J Gastroenterol 2005;100:2551–2559)

INTRODUCTION

The pathogenesis of fulminant hepatic failure (FHF) has not been profoundly defined, although several hypotheses, including those on the roles of tumor necrosis factor-α (TNF-α) (1), viral mutation (2), disturbance of the hepatic microcirculation (3), and apoptosis (4), have been presented and discussed. The significance of apoptosis via the Fas–Fas ligand (Fas–FasL) system has been the focus of studies in experimental models (5, 6) and in the clinical setting (7, 8). Intraperitoneal administration of agonistic anti-Fas antibody (Jo-1) in mice results in rapid killing with severe liver damage, as occurs in FHF (5). Hepatocyte apoptosis has been demonstrated in patients with FHF (4, 8), and although hepatocytes have been shown to express Fas (4, 7, 8) there have been no reports specifying which cells express FasL in the livers of patients with FHF. Although T-lymphocytes express FasL and play important roles in patients with chronic viral hepatitis (7, 9), there is a definite difference in the clinical features of patients with chronic hepatitis (CH) and those with FHF.

We verified the occurrence of hepatocyte apoptosis in the explanted livers of patients with FHF who underwent liver transplantation. In addition, we determined which cells (*i.e.*, macrophages and/or lymphocytes) expressed FasL. The aim of our clinical investigation was to elucidate the pathogenesis of FHF, with the ultimate aim of improving the treatment for this devastating condition.

METHODS

Patients

Our subjects were 24 patients with FHF who underwent living donor liver transplantation at Shinshu University between 1993 and 2003. Patient profiles are shown in Table 1. The definition of FHF was based on the findings of a previous report by Bernuau *et al.* (10), and the criteria adopted by King's College Hospital (11) were used as indications for liver transplantation. The causes of FHF were non-A, non-B, and non-C hepatitis in 16 patients, hepatitis B in 5, and idiosyncratic drug reaction in 3.

Liver Tissues

All tissues examined were obtained from explanted livers during liver transplantation. In addition, we examined liver tissues from nine patients with CH (liver tissue was obtained

Table 1. Profiles of Patients with Fulminant Hepatic Failure

Patient	Age	Gender	Etiology	Total Bilirubin (mg/dL)	Prothrombin Time (%)	Coma Grade
1	15 yr	M	Drug	17.8	16.0	4
2	4 yr	F	NANBNC	12.1	36.0	3
3	5 months	M	Hepatitis B	34.5	25.0	2
4	11 yr	M	NANBNC	11.8	40.0	2
5	6 yr	F	NANBNC	10.8	17.0	4
6	1 yr	F	NANBNC	6.4	7.0	3
7	18 yr	F	NANBNC	38.8	21.0	3
8	7 yr	M	NANBNC	24.5	33.0	2
9	36 yr	F	Drug	29.4	13.0	4
10	1 yr	M	NANBNC	13.9	12.0	3
11	6 months	M	NANBNC	9.3	18.0	4
12	23 yr	F	NANBNC	17.2	17.0	3
13	6 months	F	NANBNC	29.5	5.0	3
14	23 yr	F	Hepatitis B	10.3	6.7	4
15	1 yr	M	NANBNC	15.2	10.0	3
16	4 months	F	NANBNC	14.9	11.1	2
17	35 yr	F	NANBNC	16.9	13.0	4
18	44 yr	F	Hepatitis B	17.3	22.4	3
19	19 yr	M	NANBNC	28.2	12.0	3
20	9 yr	M	NANBNC	25.8	14.0	4
21	41 yr	M	Hepatitis B	24.9	27.0	4
22	20 yr	F	Hepatitis B	6.2	15.0	4
23	8 months	M	NANBNC	21.2	28.0	2
24	42 yr	F	Drug	9.0	40.6	3

NANBNC: non-A, non-B, and non-C hepatitis.

from noncancerous parts of the hepatectomized liver in cases of chronic hepatitis complicated by hepatocellular carcinoma, and informed consent for additional use of the samples was obtained) and from six living liver donors (LD) (liver tissue was obtained for histological assessment of the liver grafts and informed consent for additional use of the samples was obtained). The causes of the CH were hepatitis C in four, non-A, non-B, and non-C hepatitis in four, and hepatitis B in one. Informed consent was obtained from each patient, and the study was approved by the ethics committee of Shinshu University.

Each specimen was fixed in buffered formalin solution and embedded in paraffin wax. Serial sections (4–5 μm) were cut and mounted on clear silicon-coated glass slides (Dako, Tokyo, Japan). Ten specimens randomly selected from these 24 patients with FHF were obtained and were frozen in liquid nitrogen and stored at −80°C until use.

TUNEL Staining

To detect cells undergoing apoptosis, histological sections were stained by the terminal deoxynucleotidyl transferase (TdT)-mediated dUTP-biotin nick-end labeling (TUNEL) procedure, with some modifications as described previously (12, 13). We counted the number of TUNEL-positive cells in high-powered fields (×200) of liver tissues. The number of TUNEL-positive cells was calculated as the mean of 10 views of each liver tissue.

Immunohistochemistry

Immunohistochemical stainings for Fas, FasL, CD68, and CD8 were performed on serial hepatic tissue sections using a Dako LSAB kit (Dako). For antigen retrieval, microwave irradiation in 0.01-M citric acid buffer (pH 6.0) (for Fas and CD68) or Tris–citrate EDTA (pH 8.0) (for CD8) was carried out before application of the primary antibodies. The primary antisera used were mouse anti-Fas monoclonal antibody (ZB-4, MBL, Nagoya, Japan), rabbit anti-FasL polyclonal antibody (Nichirei, Tokyo, Japan), mouse anti-CD68 monoclonal antibody (KP1, Dako), and mouse anti-CD8 monoclonal antibody (C8/144B, Dako).

The histopathology of the liver was examined after hematoxylin and eosin staining, and the expression of each antigen was evaluated by counting the number of positive cells in high-power fields (×200) of the liver tissues. The number of positive cells was determined as the mean value of 10 views of each liver tissue specimen, with duplicate measurements.

Double Immunofluorescence Staining

Co-localization of FasL and other markers such as CD8, CD68, and hepatocytes was examined using double immunofluorescence staining methods. Mouse monoclonal antibody, OCH1E5, specific for hepatocytes was purchased from Dako. For antigen retrieval, we performed microwave irradiation in 0.01-M citric acid buffer (pH 6.0) (for FasL/CD68 as well as FasL/hepatocyte double staining) or Tris–citrate EDTA (pH 8.0) (for FasL/CD8 double staining). Tissue sections were reacted with each pair of primary antibodies, *i.e.*, FasL and CD68, FasL and CD8, and FasL and hepatocyte. Immunoreaction was detected by using a set of secondary antibodies: goat anti-rabbit IgG conjugated with rhodamine for FasL and goat anti-mouse IgG conjugated with FITC

for CD8, CD68, and hepatocyte antigen (Beckman Coulter, Tokyo, Japan).

The stained sections were mounted with Vectashield Hard Set mounting medium (Vector, Burlingame, CA, USA) and observed under an LSM 510 META laser scanning confocal microscope (Carl Zeiss, Tokyo, Japan). We calculated the number of positive cells in a sample as the mean of the counts in six fields of view (×200). Negative control experiments, in which the primary antibodies were replaced by the same host's serum, consistently showed no staining (data not shown).

RNA Extraction by Reverse Transcription PCR (RT-PCR)

Analysis of mRNA expression was performed in 10 randomly selected samples from patients with FHF and in two randomly selected samples from LD. Liver tissue was homogenized with a liquid-nitrogen-cooled mortar and pestle; the RNA was isolated by guanidium isothiocyanate and acid-phenol extraction (14). The RNA pellet was washed in 75% ethanol and resuspended in 20 μL of diethylpyrocarbonate treated with autoclaved Tris-citrate EDTA. RNA (2 μg) was reverse transcribed to cDNA by a SuperScript II first-strand synthesis system with oligo dT primer (Invitrogen Co., Carlsbad, CA, USA) and amplified using primers for human Fas; FasL; interferon-γ (IFN-γ); interferon-γ receptor α (IFN-γ Rα); interleukin-18 (IL-18); macrophage inhibitory protein 1β (MIP-1β); regulated upon activation, normal T cell expressed and secreted (RANTES); and β-actin (Table 2). PCR was performed, using Ex Taq DNA polymerase (Takara, Otsu, Japan) for 40 cycles, as follows: 94°C for 60 s (dissociation), 65°C (FasL) or 55°C (the others) for 30 s (annealing), and 72°C for 2 min (primer extension). Amplicons were visualized by 1.5% agarose gel electrophoresis.

Statistics

All data were expressed as means ± SEM. Statistical analyses were evaluated by Mann-Whitney's U-test using StatView software (SAS Institute Inc., Cary, NC, Version 5.0). Differences were designated as significant at $p < 0.05$.

RESULTS

Histological Characteristics of the FHF Liver

Although most hepatocytes had been lost and many hepatic lobules destroyed in the FHF liver, sinusoidal endothelial cells were present and dense mononuclear cells were observed (Fig. 1). In 15 of the 24 FHF patients, the remaining or regenerated hepatocytes were observed in islet formations that were sharply delimited by dense mononuclear cells. In the other 9 FHF patients, small numbers of hepatocytes were detected as pseudo bile ducts surrounded by many mononuclear cells. A large proportion of the mononuclear cells was lymphocytes and macrophages.

Apoptosis in the FHF Liver

To investigate whether apoptotic cells were present in the FHF liver, we examined DNA fragmentation as a marker of the presence of apoptotic cells by TUNEL staining of liver tissues obtained from the 24 FHF patients. Surviving hepatocytes were stained positively by TUNEL staining. The TUNEL-positive cells were present in the marginal zones of the surviving islets of hepatocytes (Fig. 2). The number of TUNEL-positive cells in the FHF liver was significantly greater than that in the CH liver or in the LD liver (Fig. 2).

Expression of Fas and FasL in Liver Tissue

The immunohistochemical studies revealed prominent staining for Fas on the surfaces and/or in the cytoplasm of hepatocytes in the FHF liver (Fig. 3). Lower levels of Fas staining were seen on the cell membranes and/or cytoplasm in the CH liver, and Fas staining in the LD liver was slight. Results of the Fas-positive hepatocyte count are shown in Figure 3.

Table 2. Genes and Primer Sequences in Reverse Transcription PCR Analysis

Gene	Primer Sequences	Amplification (bp)
Fas	5′CAG AAC TTG GAA GGC CTG CAT C3′ 5′TCT GTT CTG CTG TGT CTT GGA C3′	682
FasL	5′GGA TTG GGC CTG GGG ATG TTT CA3′ 5′TTG TGG CTC AGG GGC AGG TTG TTG3′	344
IFN-γ	5′GCA TCG TTT TGG GTT CTC TTG GCT GTT ACT GC3′ 5′CTC CTT TTT CGC TTC CCT GTT TTA GCT GCT GG3′	427
IFN-γ Rα	5′GCT GTA TGC CGA GAT GGA AAA3′ 5′AGG AAA ATG GCT GGT ATG ACG3′	588
IL-18	5′GCT TGA ATC TAA ATT ATC AGT C3′ 5′GAA GAT TCA AAT TGC ATC TTA T3′	342
MIP-1β	5′ACC CTC CCA CCG CCT GCT GC3′ 5′GTT CCA GGT CAT ACA CGT ACT CC3′	188
RANTES	5′ACC ACA CCC TGC TGC TTT GC3′ 5′CCG AAC CCA TTT CTT CTC TGG3′	159
β-actin	5′ACT ACC TCA TGA AGA TCC TCA3′ 5′CAG GAG GAG CAA TGA TCT TGA3′	441

FasL = Fas ligand; IFN-γ = interferon-γ; IFN-γ Rα = interferon-γ receptor α; IL-18 = interleukin-18; MIP-1β = macrophage inhibitory protein-1β; RANTES = regulated upon activation, normal T cell expressed and secreted.

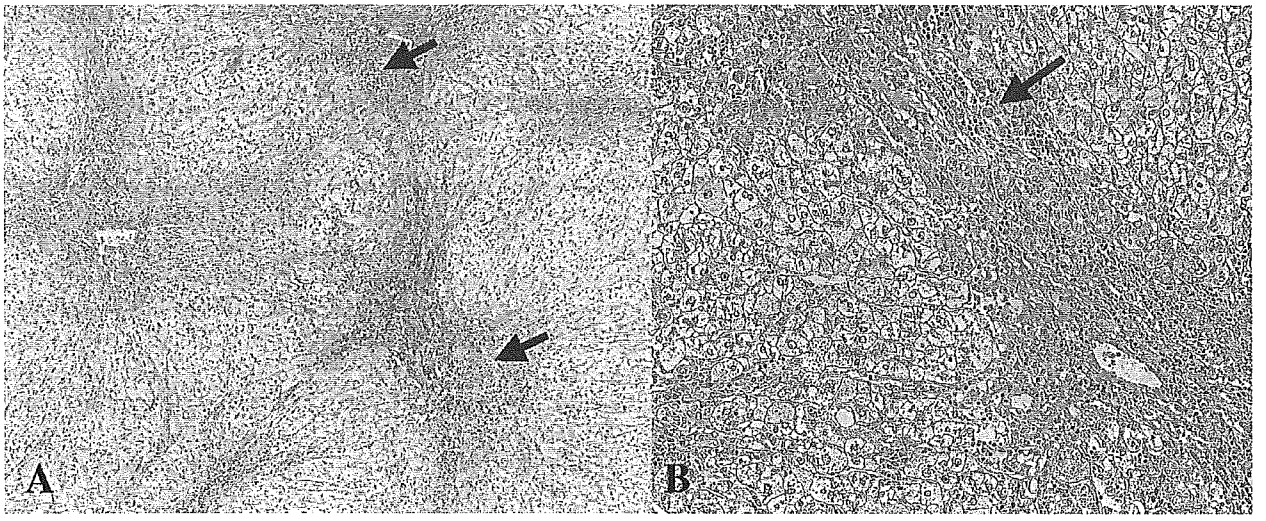

Figure 1. Representative histology of remaining hepatic lobules from a patient with FHF (Case 12). (*A*) Remaining hepatic lobules are composed of degenerating hepatocytes showing marked ballooning. The collapsed intervening parenchyma is visible among the lobules (arrows) (original magnification, ×20). With the orcein stain, the collapsed area contains no demonstrable elastic fibers. (*B*) Large numbers of inflammatory mononuclear cells surround the hepatic lobules (arrow). (Hematoxylin-eosin staining; original magnification, ×100)

FasL was stained predominantly on mononuclear cells around the margins of the hepatocyte islets (Fig. 4). The number of cells staining positively for FasL was significantly greater in the FHF liver than in the CH and LD livers.

Macrophage and Cytotoxic T-Cell Infiltration of FHF Liver

To identify the nature of the mononuclear cells, we immunostained the FHF liver tissues using anti-CD68 antibody as a marker of macrophages and anti-CD8 antibody as a marker of cytotoxic T cells. Enlarged CD68-positive cells were present around the damaged hepatocyte islets in the FHF liver (Fig. 5). Enlarged CD68-positive cells were present around the pseudolobules in the CH liver (data are not shown). In the LD liver, CD68-positive cells were observed only in the sinusoids. CD8-positive cells were found in similar locations in the FHF (Fig. 6) and CH livers. There was no significant difference in the count of CD8-positive cells between the FHF liver and the CH liver.

Cellular Localization of FasL

To characterize the cells expressing FasL in the FHF liver, we performed double immunofluorescence staining using CD68 or CD8 or anti-hepatocyte antibody and FasL (Fig. 7). There were significantly more CD68-positive cells co-expressing FasL in the FHF liver (41.71 ± 8.99/hpf) (Fig. 7A) than in the CH liver (0.79 ± 0.21/hpf) (Fig. 7C) ($p < 0.0002$). In contrast, there were significantly fewer CD8-positive cells co-expressing FasL in the FHF liver (1.18 ± 0.22/hpf) (Fig. 7B) than in the CH liver (6.32 ± 2.56/hpf) (Fig. 7D) ($p < 0.0001$). No hepatocytes expressed FasL (Fig. 7E).

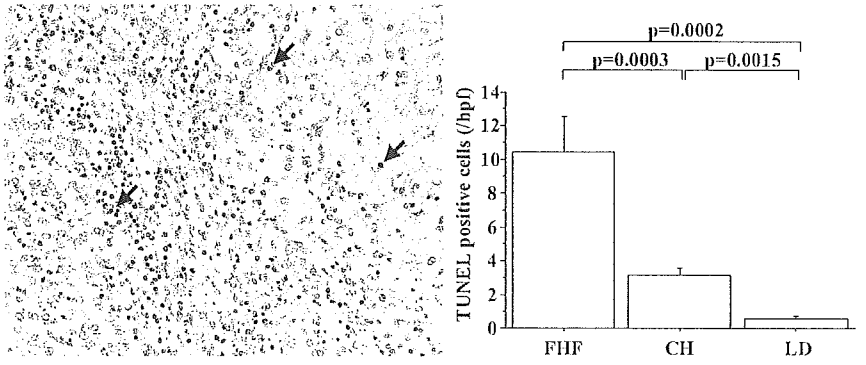

Figure 2. TUNEL staining of FHF liver tissue (Case 12). TUNEL-positive hepatocytes are found at the periphery of the remaining hepatic lobules (arrows), and inflammatory mononuclear cells being adjacent to them (original magnification, ×200). The numbers of TUNEL-positive cells were 10.45 ± 2.12/hpf, 2.77 ± 0.40/hpf, and 0.57 ± 0.14/hpf in the FHF, CH, and LD liver tissues, respectively.

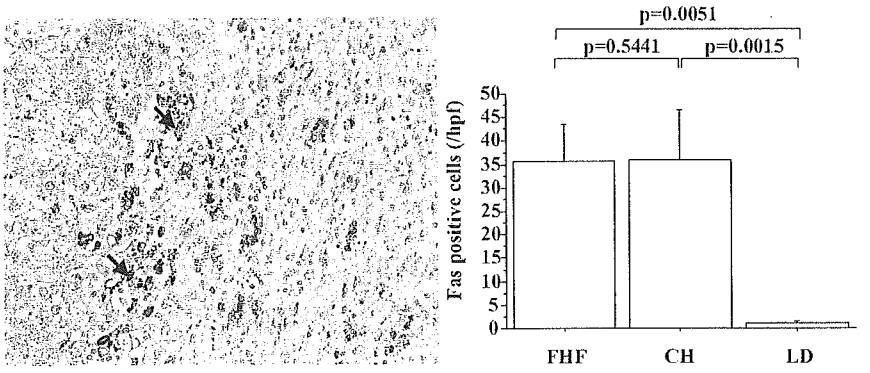

Figure 3. Representative immunohistochemistry of Fas in the FHF liver (Case 12). Fas is largely expressed by injured hepatocytes located in the marginal zones of the remaining hepatic lobules (arrows) (original magnification, ×200). Note that Fas is expressed in the cytoplasm of the hepatocytes. The numbers of Fas-positive cells were 35.76 ± 7.63/hpf, 23.22 ± 5.70/hpf, and 1.13 ± 0.38/hpf in the FHF, CH, and LD livers, respectively.

Semi-Quantitative Analysis of Cytokines and Chemokines in the FHF Liver

We performed semi-quantitative RT-PCR to evaluate mRNA expression of cytokines and chemokines in the FHF liver (Fig. 8). In the livers of seven patients with FHF, the mRNAs of FasL, IFN-γ, IL-18, MIP-1β, and RANTES were expressed more strongly than in the LD liver. Both the FHF liver and the LD liver showed expression of the mRNAs of Fas and IFN-γ Rα.

DISCUSSION

We verified the occurrence of hepatocyte apoptosis in the livers of FHF patients who underwent liver transplantation. In addition, we found that up-regulation of FasL occurred in most of the FHF liver and that the cells that expressed FasL were macrophages, not cytotoxic lymphocytes. Macrophages and their expression of FasL may play roles in the pathogenesis of FHF. These observations were different from those in the CH liver, especially in terms of the roles of cytotoxic lymphocytes. This is the first description of the cells in charge of FasL expression in FHF.

Although the pathogenesis of FHF has not been fully defined, the involvement of IFN and chemokines in the pathogenesis of FHF has been suggested in experimental models (15, 16) and in clinical studies (17, 18). Considering the potent proinflammatory functions of IFN, an unbalanced activation of the immune system caused by IFN plays a pivotal role in the pathogenesis of FHF (17). The main source of IFN is considered Kupffer cells, infiltrating macrophages, and lymphocytes (17). In addition, chemokines of the CC class are of particular interest in FHF, because they attract and activate macrophages and T-lymphocytes, the cellular hallmark of the intrahepatic infiltrates in this disease. Leifeld *et al.* (18) analyzed the role of CC-chemokines in the pathogenesis of FHF by examining serum levels and intrahepatic expression of monocyte chemoattractant protein-1, MIP-1α, MIP-1β, and RANTES in the livers and sera of patients with FHF and controls. Serum levels and intrahepatic expression of all chemokines studied in FHF exceeded the levels in chronic

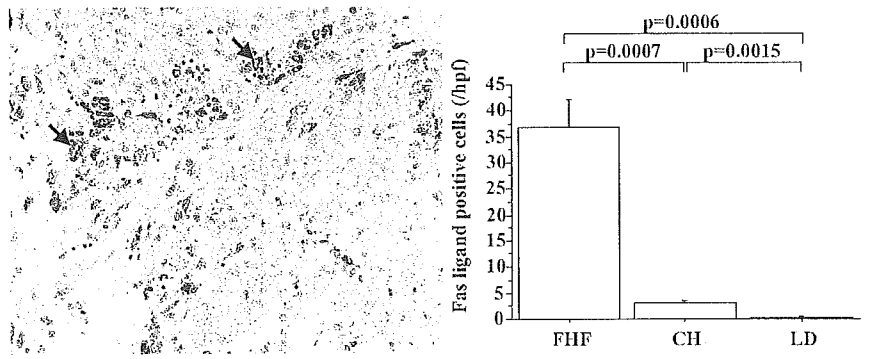

Figure 4. Representative immunohistochemistry of FasL in the FHF liver (Case 12). FasL is expressed by the inflammatory mononuclear cells infiltrating the marginal zones of the remaining hepatic lobules (arrows) (original magnification, ×200). Note that FasL is expressed in the entire cytoplasm of the mononuclear cells being adjacent to the injured hepatocytes. The numbers of FasL positive cells were 36.84 ± 5.30/hpf, 2.50 ± 0.55/hpf, and 0.30 ± 0.15/hpf in the FHF, CH, and LD liver tissues, respectively.

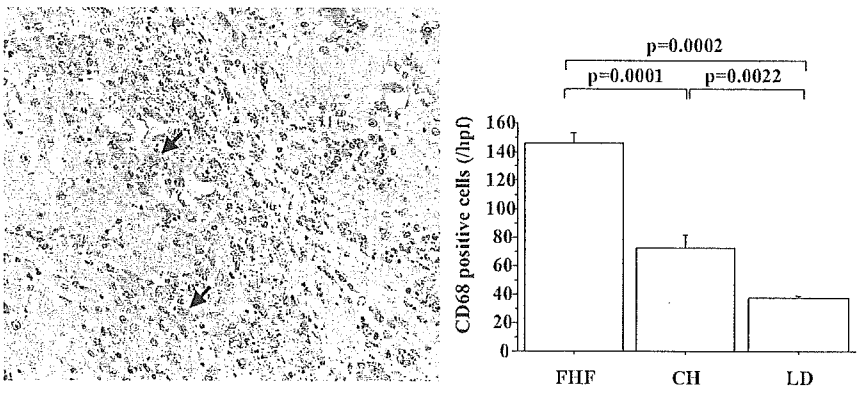

Figure 5. Representative immunohistochemistry of CD68 in the FHF liver (Case 18). CD68 is expressed in the macrophages infiltrating the remaining hepatic lobules (arrows) (original magnification, ×200).The numbers of CD68-positive cells were 145.68 ± 7.61/hpf, 60.45 ± 0.35/hpf, and 37.88 ± 1.61/hpf in the FHF, CH, and LD liver tissues, respectively.

liver diseases and normal controls (18). In fulminant hepatitis B, it has been indicated that massive induction of the proinflammatory cytokines IL-12 and IFN-γ is apparently not counterbalanced by the anti-inflammatory cytokine IL-10 (19). This cytokine imbalance may play an important role in promoting inflammatory reactions leading to massive liver damage in fulminant hepatitis B. Meanwhile, in chronic hepatitis C, Nischalke *et al.* (20) supported a correlation of the intrahepatic expression of the CC chemokine RANTES and the degree of periportal and portal inflammatory liver damage. The results of our RT-PCR study of liver tissue showed increased expression of FasL, IFN-γ, IL-18, MIP-1β, and RANTES in the FHF liver but not in the LD liver. These cytokines and chemokines may play roles in the pathogenesis of FHF. Hepatic macrophages have been shown to be responsible for IL-18 production in response to antigen stimulation (21). It has been suggested that activated hepatic macrophages produce IL-18 and then enhance IFN-γ production by CD8-positive T-lymphocytes, producing massive hepatic necrosis as well as virus elimination in FHF (22). IFN-γ has been shown to induce hepatocyte apoptosis through multiple pathways, including the Fas–FasL system, in an experimental setting using the Con-A hepatitis model in mice (23). Muschen *et al.* reported that administration of IFN-γ mediates FasL mRNA expression by rat Kupffer cells rather than by hepatic parenchymal cells or hepatic T-lymphocytes (24). RANTES has been shown to regulate the expression of FasL in HIV-specific cytotoxic T-cells followed by the killing of target cells by apoptosis (25). RANTES and MIP-1β expression leads to uncontrolled recruitment and activation of inflammatory cells—especially macrophages and cytotoxic lymphocytes—as an early step in the pathogenesis of FHF (18). In this clinical study, because of the ethical reasons, liver specimens were obtained at one point (at the time of liver transplantation) in the course of FHF. Taking into account the putative multistep pathogenesis as well as considerably redundant involvement of the chemokines in FHF, it is difficult to clearly assess the relevance of these cytokines and chemokines.

In terms of hepatocyte apoptosis in FHF, hepatocytes have been shown to express Fas, and the role of hepatocyte apoptosis that occurs via the Fas–FasL system has been the focus of some studies (6–9). However, no reports have specified which cells express FasL in the livers of patients with FHF.

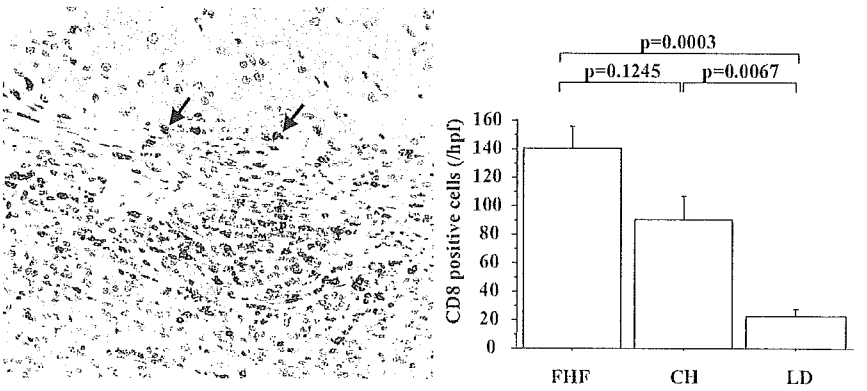

Figure 6. Immunohistochemistry of CD8 in the FHF liver (Case 9). Cytotoxic T cells positive for CD8 can be seen around the remaining hepatic lobules (arrows) (original magnification, ×200). The numbers of CD8-positive cells were 139.75 ± 16.22/hpf, 114.60 ± 15.70/hpf, and 22.62 ±5.04/hpf in the FHF, CH, and LD liver tissues, respectively.

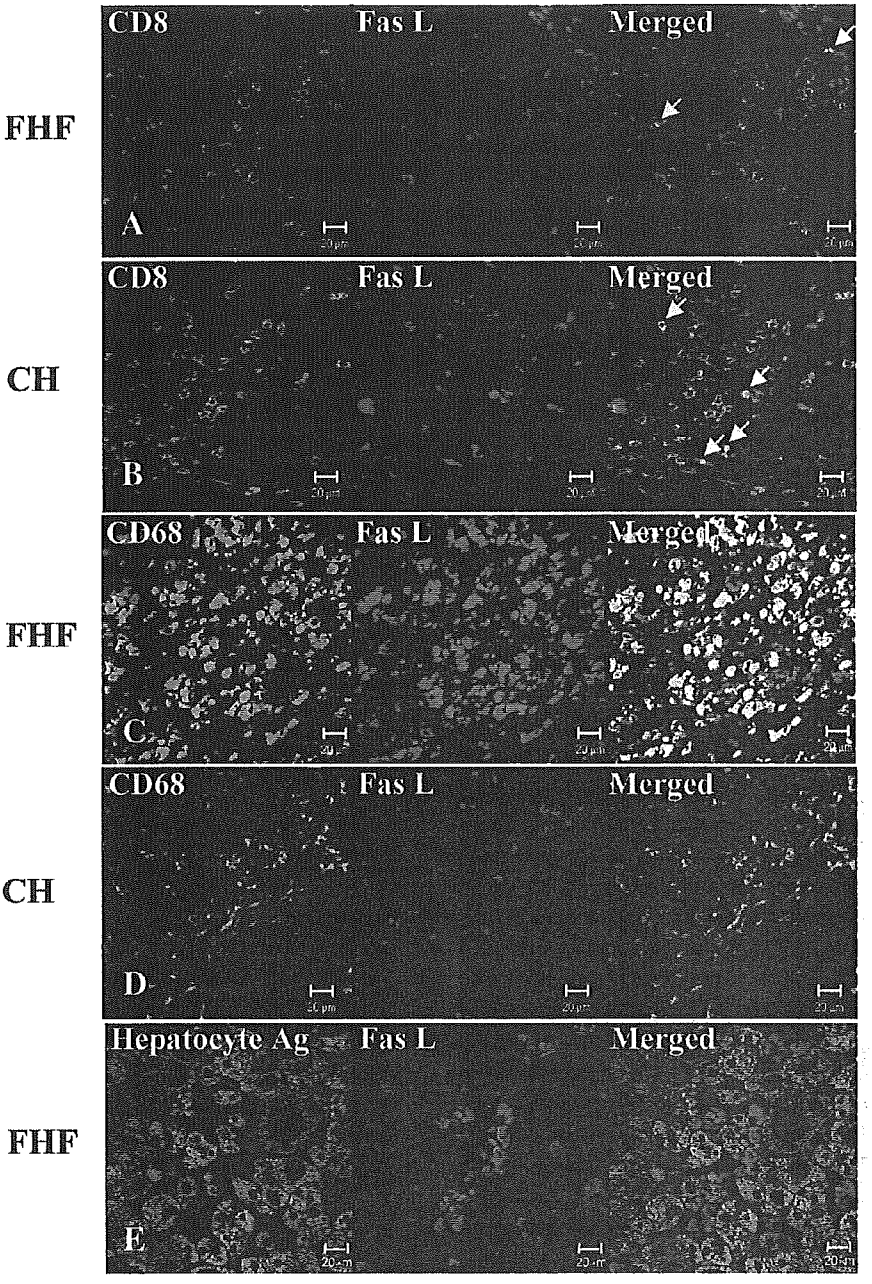

Figure 7. Double immunohistochemistry of FasL and other markers—CD8, CD68, and hepatocyte antigen—in FHF (Case 14) and CH (type B) livers. FasL-positive cells are indicated in red (middle column), and other markers are indicated in green (left column). Yellow coloration of the merged figures indicates double-positive cells (right column). (*A*) Cells double-positive for both FasL and CD8 were rarely detected in the FHF liver (arrows). (*B*) Cells double-positive for both FasL and CD8 were observed more frequently in the CH liver (arrows) than in the FHF liver. (*C*) Cells double-positive for both FasL and CD68 were observed frequently in the FHF liver. The small cells that are FasL+ and CD68− are red blood cells. (*D*) Few cells double-positive for both FasL and CD68 were detected in the CH liver. (*E*) FasL was not expressed in the hepatocytes, because cells positive for both FasL and hepatocyte antigen were not detected in the FHF liver.

We verified the occurrence of hepatocyte apoptosis in the explanted livers of patients with FHF who underwent liver transplantation and double immunofluorescence staining showed that FasL was expressed predominantly on liver macrophages. Fas is up-regulated in the hepatocytes of patients with various liver diseases, such as chronic hepatitis B (26), hepatitis C (27), alcoholic liver disease (28), Wilson's disease (29), and FHF (4, 7, 8). FasL has been shown to mediate hepatocyte apoptosis in mainly the initial stage of development of viral hepatitis (30). The fact that the localizations of TUNEL-positive cells, Fas-positive hepatocytes, and FasL-positive macrophages were similar, strongly suggests that

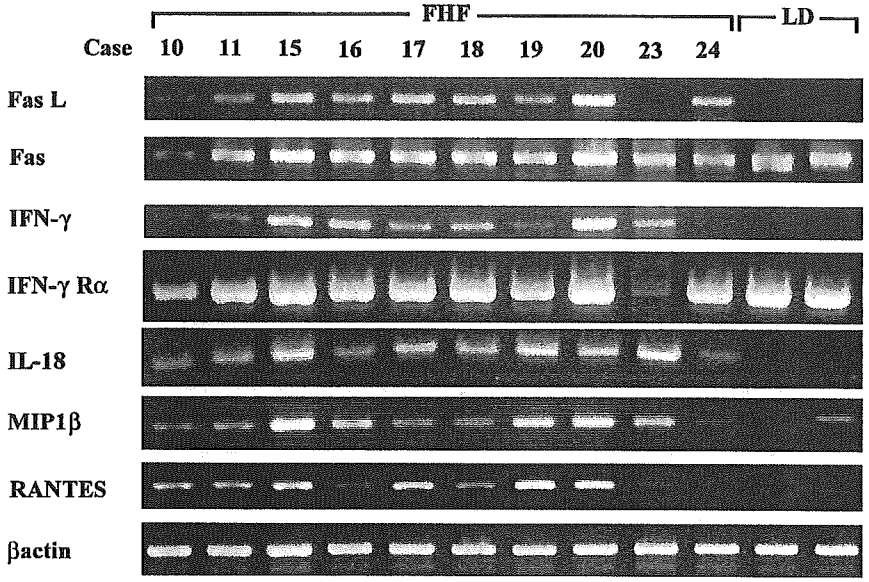

Figure 8. Semi-quantitative RT-PCR of cytokine and chemokine in the FHF and LD liver. The mRNA of the receptors such as Fas and IFN-γ Rα was expressed both in the FHF and LD liver. In contrast, mRNAs of Fas L, IFN-γ, IL-18, MIP-1β, and RANTES were expressed strongly in seven cases with FHF compared with the LD liver.

Fas–FasL-mediated apoptosis occurred in the FHF liver. FasL was expressed predominantly on liver macrophages but rarely on CD8-positive lymphocytes. These findings were different from those of CH livers, in which FasL was expressed mainly on CD8-positive lymphocytes and rarely on hepatic macrophages. Our observations in the CH liver accord with those of previous reports of CH in humans and in experimental liver injury (7, 9, 30–32). The increased number of macrophages but not of cytotoxic lymphocytes in the FHF liver compared with the CH liver is notable. This clinical finding is important for identifying the pathological difference between FHF and CH. In CH group, when compared between hepatitis C subgroup and non-A, non-B, and non-C subgroups, the above described findings were similar. Several reports have described the significance of FasL-positive liver macrophages in apoptosis of cells lining the intrahepatic bile ducts in primary biliary cirrhosis (33) and in hepatocyte apoptosis in hepatitis B (32). Ryo *et al.* reported FasL mRNA expression by lymphocytes in the liver in FHF (8), but our results did not confirm their finding.

Considering that activation of infiltration macrophages to the liver play pivotal roles in the pathogenesis of FHF (*e.g.*, mediating immune-mediated liver cell damage, chemokine network, and apoptosis), further investigation to establish a strategy to get macrophages under control during FHF needs to be formulated.

In summary, this clinical study suggests that hepatic macrophages play a role in the pathogenesis of FHF via FasL expression. Although the disease no doubt has a multifaceted pathogenesis, down-regulation of activated hepatic macrophages could be a useful strategy in the treatment of human FHF.

Reprint requests and correspondence: Yasuhiko Hashikura, M.D., Department of Surgery, Shinshu University School of Medicine, 3-1-1 Asahi, Matsumoto 390-8621, Japan.

Received January 7, 2005; accepted June 6, 2005.

REFERENCES

1. Streetz K, Leifeld L, Grundmann D, et al. Tumor necrosis factor alpha in the pathogenesis of human and murine fulminant hepatic failure. Gastroenterology 2000;119:446–60.
2. Sato S, Suzuki K, Akahane Y, et al. Hepatitis B virus strains with mutations in the core promoter in patients with fulminant hepatitis. Ann Intern Med 1995;122:241–8.
3. Hirata K, Ogata I, Ohta Y, et al. Hepatic sinusoidal cell destruction in the development of intravascular coagulation in acute liver failure of rats. J Pathol 1989;158:157–65.
4. Kasahara I, Saitoh K, Nakamura K. Apoptosis in acute hepatic failure: Histopathological study of human liver tissue using the tunel method and immunohistochemistry. J Med Dent Sci 2000;47:167–75.
5. Ogasawara J, Watanabe-Fukunaga R, Adachi M, et al. Lethal effect of the anti-Fas antibody in mice. Nature 1993;364:806–9.
6. Tagawa Y, Kakuta S, Iwakura Y. Involvement of Fas/Fas Ligand system-mediated apoptosis in the development of concanavalin A-induced hepatitis. Eur J Immunol 1998;28:4105–13.
7. Galle PR, Hofmann WJ, Walczak H, et al. Involvement of the CD95 (APO-1/Fas) receptor and ligand in liver damage. J Exp Med 1995;182:1223–30.
8. Ryo K, Kamogawa Y, Ikeda I, et al. Significance of Fas antigen-mediated apoptosis in human fulminant hepatic failure. Am J Gastroenterol 2000;95:2047–55.
9. Ono K, Tanaka Y, Kusano F, et al. Fas-Ligand and perforin expression in infiltrating cytotoxic T lymphocytes in the liver of chronic hepatitis C. Hepatol Res 2002;23:153–62.

10. Bernuau J, Rueff B, Benhamou JP. Fulminant and subfulminant liver failure: Definitions and causes. Semin Liver Dis 1986;6:97–106.
11. O'Grady JG, Alexander GJ, Hayllar KM, et al. Early indicators of prognosis in fulminant hepatic failure. Gastroenterology 1989;97:439–45.
12. Gavrieli Y, Sherman Y, Ben-Sasson SA. Identification of programmed cell death in situ via specific labeling of nuclear DNA fragmentation. J Cell Biol 1992;119:493–501.
13. Soeda J, Miyagawa S, Sano K, et al. Cytochrome c release into cytosol with subsequent caspase activation during warm ischemia in rat liver. Am J Physiol Gastrointest Liver Physiol 2001;281:G1115–23.
14. Chomczynski P, Sacchi N. Single-step method of RNA isolation by acid guanidinium thiocyanate-phenol-chloroform extraction. Anal Biochem 1987;162:156–9.
15. Ferreira AM, Rollins BJ, Faunce DE, et al. The effect of MCP-1 depletion on chemokine and chemokine-related gene expression: Evidence for a complex network in acute inflammation. Cytokine 2005;30:64–71.
16. Iwaki T, Sugimura M, Nishihira J, et al. Recombinant adenovirus vector bearing antisense macrophage migration inhibitory factor cDNA prevents acute lipopolysaccharide-induced liver failure in mice. Lab Invest 2003;83:561–70.
17. Leifeld L, Ramakers J, Schneider AM, et al. Intrahepatic MxA expression is correlated with interferon-alpha expression in chronic and fulminant hepatitis. J Pathol 2001;194:478–83.
18. Leifeld L, Dumoulin FL, Purr I, et al. Early up-regulation of chemokine expression in fulminant hepatic failure. J Pathol 2003;199:335–44.
19. Leifeld L, Cheng S, Ramakers J, et al. Imbalanced intrahepatic expression of interleukin 12, interferon gamma, and interleukin 10 in fulminant hepatitis B. Hepatology 2002;36:1001–8.
20. Nischalke HD, Nattermann J, Fischer HP, et al. Semiquantitative analysis of intrahepatic CC-chemokine mRNAs in chronic hepatitis C. Mediators Inflamm 2004;13:357–9.
21. Munder M, Mallo M, Eichmann K, et al. Murine macrophages secrete interferon γ upon combined stimulation with interleukin (IL)-12 and IL-18: A novel pathway of autocrine macrophage activation. J Exp Med 1998;187:2103–8.
22. Yumoto E, Higashi T, Nouso K, et al. Serum gamma-interferon-inducing factor (IL-18) and IL-10 levels in patients with acute hepatitis and fulminant hepatic failure. J Gastroenterol Hepatol 2002;17:285–94.
23. Tagawa Y, Sekikawa K, Iwakura Y. Suppression of concanavalin A-induced hepatitis in IFN-γ(-/-) mice, but not in TNF-α(-/-) mice: Role for IFN-γ in activating apoptosis of hepatocytes. J Immunol 1997;159:1418–28.
24. Muschen M, Warskulat U, Peters-Regehr T, et al. Involvement of CD95 (Apo-1/Fas) ligand expressed by rat Kupffer cells in hepatic immunoregulation. Gastroenterology 1999;116:666–77.
25. Hadida F, Vieillard V, Mollet L, et al. RANTES regulates Fas Ligand expression and killing by HIV-specific CD8 cytotoxic T cells. J Immunol 1999;163:1105–9.
26. Mochizuki K, Hayashi N, Hiramatsu N, et al. Fas antigen expression in liver tissues of patients with chronic hepatitis B. J Hepatol 1996;24:1–7.
27. Hiramatsu N, Hayashi N, Katayama K, et al. Immunohistochemical detection of Fas antigen in liver tissue of patients with chronic hepatitis C. Hepatology 1994;19:1354–9.
28. Natori S, Rust C, Stadheim LM, et al. Hepatocyte apoptosis is a pathologic feature of human alcoholic hepatitis. J Hepatol 2001;34:248–53.
29. Strand S, Hofmann WJ, Grambihler A, et al. Hepatic failure and liver cell damage in acute Wilson's disease involve CD95 (APO-1/Fas) mediated apoptosis. Nat Med 1998;4:588–93.
30. Kondo T, Suda T, Fukuyama H, et al. Essential roles of the Fas Ligand in the development of hepatitis. Nat Med 1997;3:409–13.
31. Roth E, Pircher H. IFN-gamma promotes Fas Ligand- and perforin-mediated liver cell destruction by cytotoxic CD8 T cells. J Immunol 2004;172:1588–94.
32. Tang TJ, Kwekkeboom J, Laman JD, et al. The role of intrahepatic immune effector cells in inflammatory liver injury and viral control during chronic hepatitis B infection. J Viral Hepat 2003;10:159–67.
33. Iwata M, Harada K, Hiramatsu K, et al. Fas Ligand expressing mononuclear cells around intrahepatic bile ducts co-express CD68 in primary biliary cirrhosis. Liver 2000;20:129–35.

nature immunology

N-acetylglucosamine-6-*O*-sulfotransferases 1 and 2 cooperatively control lymphocyte homing through L-selectin ligand biosynthesis in high endothelial venules

Hiroto Kawashima[1], Bronislawa Petryniak[2], Nobuyoshi Hiraoka[1], Junya Mitoma[1], Valerie Huckaby[1], Jun Nakayama[3], Kenji Uchimura[4], Kenji Kadomatsu[4], Takashi Muramatsu[4], John B Lowe[2] & Minoru Fukuda[1]

Lymphocyte homing is mediated by specific interactions between L-selectin on lymphocytes and sulfated carbohydrates restricted to high endothelial venules in lymph nodes. Here we generated mice deficient in both *N*-acetylglucosamine-6-*O*-sulfotransferase 1 (GlcNAc6ST-1) and GlcNAc6ST-2 and found that mutant mice had approximately 75% less homing of lymphocytes to the peripheral lymph nodes than did wild-type mice. Consequently, these mice had lower contact hypersensitivity responses than those of wild-type mice. Carbohydrate structural analysis showed that 6-sulfo sialyl Lewis X, a dominant ligand for L-selectin, was almost completely absent from the high endothelial venules of these mutant mice, whereas the amount of unsulfated sialyl Lewis X was much greater. These results demonstrate the essential function of GlcNAc6ST-1 and GlcNAc6ST-2 in L-selectin ligand biosynthesis in high endothelial venules and their importance in immune surveillance.

Lymphocytes encounter antigens derived from foreign pathogens and initiate immune responses in secondary lymphoid organs such as lymph nodes and Peyer's patches. Therefore, homing of lymphocyte to secondary lymphoid organs is an essential process for immune surveillance. Lymphocyte homing is critically dependent on a specific interaction between the lymphocyte-homing receptor L-selectin and its ligands, whose expression is restricted to high endothelial venules (HEVs) in the lymph nodes[1]. This adhesive interaction mediates lymphocyte tethering and rolling on the surface of HEVs, which is a prerequisite for the subsequent lymphocyte chemokine-dependent activation, integrin-mediated firm attachment to the endothelium and transmigration across blood vessels[2–5].

L-selectin is a carbohydrate-binding protein that binds to its ligands on HEVs in a calcium-dependent way. HEV-restricted ligands for L-selectin include GlyCAM-1, CD34, podocalyxin-like protein, Sgp200, endoglycan and MAdCAM-1, all of which have mucin-like domains that act as scaffolding for *O*-glycans[6]. The ability of these ligands to function entirely depends on their 'decoration' with specific carbohydrate structures, including 6-sulfo sialyl Lewis X (sialyl-α(2-3)-galactopyranosyl-β(1-4)-[fucopyranosyl-α(1-3)(sulfo-6)]-*N*-acetylglucosamine) which contains fucose, sialic acid and sulfate[6].

The pivotal function of fucosylation of L-selectin ligands for their interaction with L-selectin has been established by genetic studies of mice. Mice deficient in fucosyltransferase VII (FucT-VII) have a reduction of nearly 80% in homing of lymphocytes to the peripheral lymph nodes, indicating that FucT-VII is the principal enzyme involved in fucosylation of L-selectin ligands on HEVs[7]. Studies using mice doubly deficient in both FucT-VII and FucT-IV have demonstrated an additional function for FucT-IV in HEV ligand fucosylation[8]. The essential involvement of sialylation of L-selectin ligands has also been demonstrated by experiments showing sialidase treatment of lymph node sections completely abrogates L-selectin-dependent binding of lymphocytes to HEVs in peripheral lymph nodes[9].

Sulfation of L-selectin ligands is important in the interaction with L-selectin *in vitro*. An initial demonstration of such a requirement showed that treatment of lymph node organ culture with chlorate, an inhibitor of sulfation, abrogates interaction between recombinant L-selectin and its glycoprotein ligands[10,11]. Subsequently, the use of a specific antibody identified the main capping group of L-selectin ligands on HEVs in human lymph nodes as 6-sulfo sialyl Lewis X[12]. The HEV-restricted sulfotransferase *N*-acetylglucosamine-6-*O*-sulfotransferase-2 (GlcNAc6ST-2, also called HEC-GlcNAc6ST or L-selectin ligand sulfotransferase) has been cloned and participates in the biosynthesis of 6-sulfo sialyl Lewis X and can reconstitute the L-selectin ligand *in vitro*[13,14]. Furthermore, the 6-sulfo sialyl Lewis X structure is present in either the core 2 or extended core 1 branch or in both branches of L-selectin ligand *O*-glycans[15]. Moreover, the MECA-79 antibody[16], which is widely used to detect HEVs in lymph nodes or HEV-like vessels at the sites of chronic inflammation, recognizes *O*-glycans containing 6-sulfo *N*-acetylglucosamine in the extended

[1]Glycobiology Program, Cancer Research Center, The Burnham Institute, La Jolla 92037, California, USA. [2]Howard Hughes Medical Institute, Life Sciences Institute, University of Michigan Medical School, Ann Arbor, Michigan 48109, USA. [3]Department of Pathology, Shinshu University School of Medicine, Matsumoto 390-8621, Japan. [4]Department of Biochemistry, Nagoya University School of Medicine, Nagoya 466-8550, Japan. Correspondence should be addressed to M.F. (minoru@burnham.org).

Received 19 June; accepted 25 August; published online 9 October 2005; doi:10.1038/ni1259

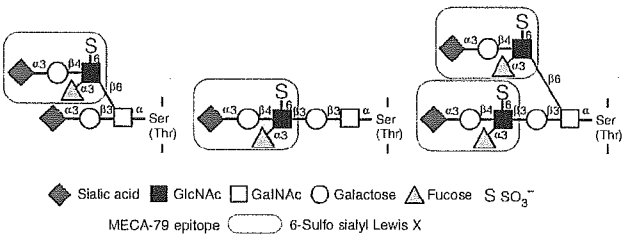

Figure 1 L-selectin ligand oligosaccharides. Core 2–branched *O*-glycan (left), extended core 1 structure (middle) and biantennary *O*-glycan containing both a core 2 branch and an extended core 1 structure (right) modified with 6-sulfo sialyl Lewis X (gray outlined areas) function as L-selectin ligand oligosaccharides in HEVs. The extended core 1 structures modified with GlcNAc-6-*O*-sulfate (yellow shaded areas) are recognized by MECA-79 (ref. 15). Each Greek character and number represents a carbohydrate linkage.

core 1 structure[15]. Although those studies have indicated a sulfation requirement of HEV-borne carbohydrates as L-selectin ligands *in vitro*, that requirement has not been demonstrated *in vivo*.

For assessment of the function of the sulfation of L-selectin ligands *in vivo*, mutant mice deficient in the HEV-restricted sulfotransferase GlcNAc6ST-2 have been generated[17,18]. In these mice, the binding of MECA-79 to lymph node HEVs is substantially diminished, except for binding in the lining of HEVs on the surface away from the lumen, suggesting that the GlcNAc-6-*O*-sulfation in the extended core 1 branch is mediated mainly by GlcNAc6ST-2. Oligosaccharide structural analysis has indicated that GlcNAc-6-*O*-sulfation in the extended core 1 structure on GlyCAM-1 is substantially less in GlcNAc6ST-2–deficient mice than in wild-type mice[17]; however, the GlcNAc-6-*O*-sulfation in the core 2–branched *O*-glycan persists in GlcNAc6ST-2–deficient mice. Consistent with that observation, there is only partial disruption of lymphocyte homing (approximately 50%) in GlcNAc6ST-2–deficient mice[17,18].

Four mouse GlcNAc-6-*O*-sulfotransferases have been identified[19,20]. GlcNAc6ST-1 is widely expressed in various tissues, including lymph node HEVs[21], and functions in L-selectin ligand biosynthesis *in vitro*[22] and *in vivo*[23]. GlcNAc6ST-1–deficient mice have a reduction of an approximately 20% in homing of lymphocytes to peripheral lymph nodes[23], suggesting that GlcNAc6ST-1 and GlcNAc6ST-2 might have overlapping or complementary functions. To determine the sulfation requirement of L-selectin ligands *in vivo* in further detail, we generated mice deficient in both GlcNAc6ST-1 and GlcNAc6ST-2 and show here that these sulfotransferases cooperatively have a chief function in L-selectin ligand biosynthesis in HEVs. Systematic carbohydrate analysis of an HEV-specific glycoprotein showed that essentially no 6-sulfo sialyl Lewis X structure was synthesized in the HEVs of mice deficient in both GlcNAc6ST-1 and GlcNAc6ST-2 ('double-knockout' mice), but that the amount of the unsulfated sialyl Lewis X structure was up to sevenfold greater than that in wild-type mice. Moreover, contact hypersensitivity responses were substantially diminished in the double-knockout mice because of a reduction in lymphocyte trafficking to the draining lymph nodes. Our study provides a link between the structural alterations of carbohydrates in HEVs and lymphocyte recruitment in health and disease.

RESULTS

Expression of L-selectin ligands in HEVs

To determine the expression of L-selectin-reactive carbohydrates in HEVs of mutant mice, we did immunofluorescence studies using MECA-79 and an L-selectin–immunoglobulin M (L-sel–IgM) chimeric protein. MECA-79 recognizes extended core 1 structures modified with GlcNAc-6-*O*-sulfate, whereas L-selectin interacts with various *O*-glycans modified with 6-sulfo sialyl Lewis X present in HEVs[15] (**Fig. 1**). Binding of MECA-79 to HEVs in peripheral lymph nodes and mesenteric lymph nodes was completely abolished in double-knockout mice (**Fig. 2a**). Only expression of enhanced green fluorescent protein (EGFP), which replaced the catalytic domain and stem region of GlcNAc6ST-2 in the targeting vector[17], was detectable in HEVs. In Peyer's patches of mice deficient in GlcNAc6ST-1 alone, MECA-79 staining was undetectable, consistent with published results[23]. In contrast, the binding of L-sel–IgM to HEVs of peripheral lymph nodes and mesenteric lymph nodes was not completely abolished in the double-knockout mice, although it was substantially reduced relative to that of wild-type mice or mice deficient in either GlcNAc6ST-1 or GlcNAc6ST-2 (**Fig. 2b**). These results indicated that GlcNAc-6-*O*-sulfation in the extended core 1 branch of *O*-glycans was

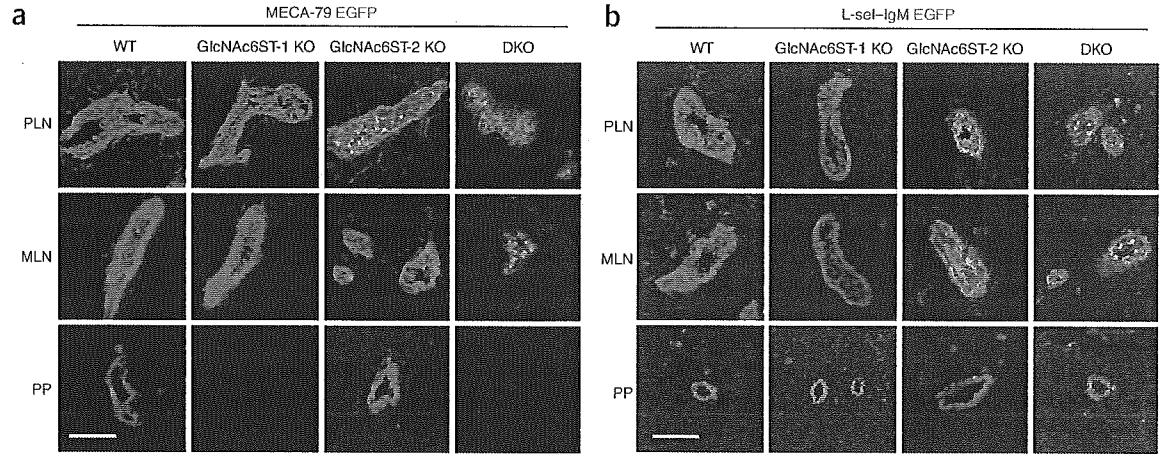

Figure 2 Expression of MECA-79 antigen, L-selectin ligands and the GlcNAc6ST-2–EGFP chimeric protein. Frozen sections (7 μm in thickness) of peripheral lymph nodes (PLN), mesenteric lymph nodes (MLN) and Peyer's patches (PP) from wild-type (WT), GlcNAc6ST-1–deficient (GlcNAc6ST-1 KO), GlcNAc6ST-2–deficient (GlcNAc6ST-2 KO) and double-knockout (DKO) mice were stained with MECA-79 (red in **a**) or L-sel–IgM (red in **b**). Green fluorescence is from the GlcNAc6ST-2–EGFP chimeric protein[17]. Scale bars, 50 μm. Data are representative of ten independent experiments.

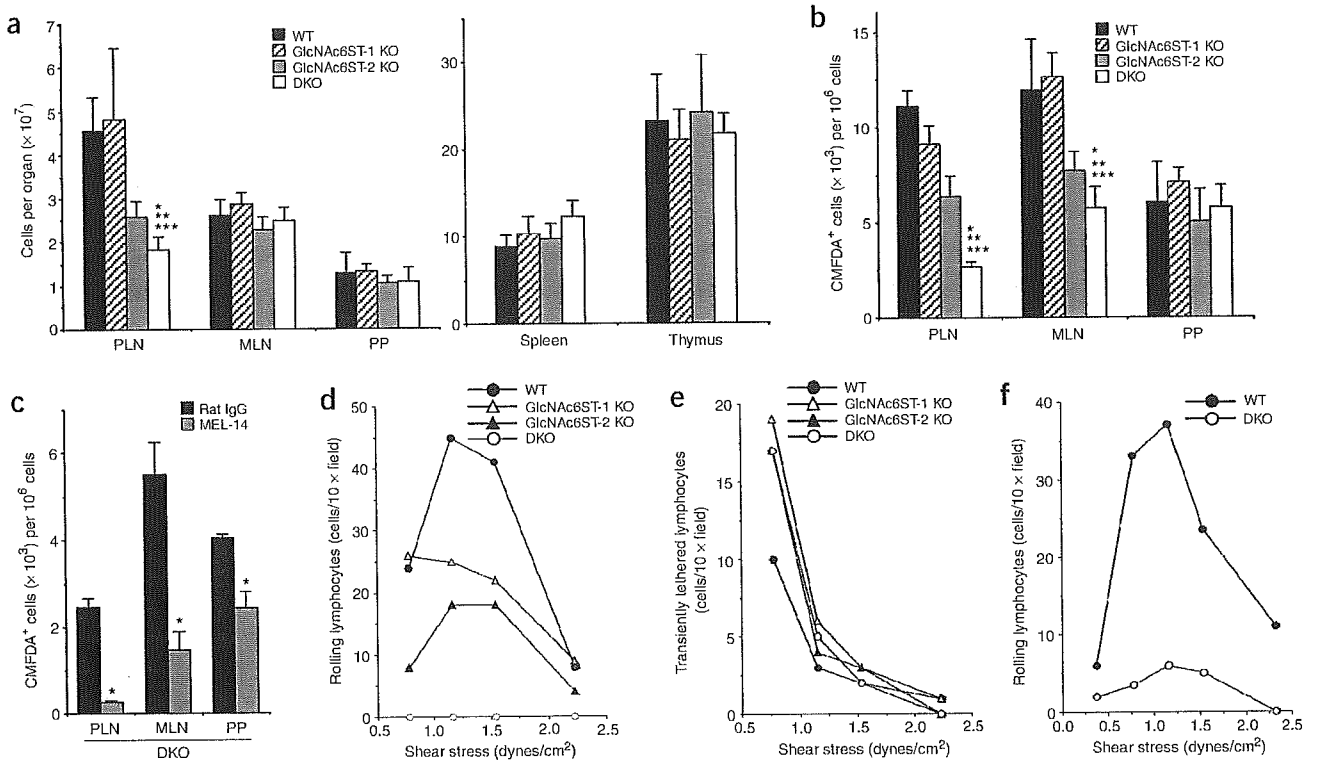

Figure 3 Lymphocyte trafficking to secondary lymphoid organs. (**a**) Lymphocytes recovered from lymphoid organs of 7-week-old wild-type and null mice ($n = 5$–7 mice). *, $P < 0.01$, versus wild-type mice; **, $P < 0.01$, versus GlcNAc6ST-1-deficient mice; ***, $P < 0.02$, versus GlcNAc6ST-2-deficient mice. (**b**,**c**) Flow cytometry of lymphocytes in lymphoid organs. CMFDA-labeled lymphocytes (2.5×10^7 cells) were injected into tail veins of wild-type and null mice (**b**) or CMFDA-labeled lymphocytes (2.5×10^7 cells) incubated with 30 μg of MEL-14 (rat IgG2a) or rat IgG were injected into tail veins of double-knockout mice (**c**). Then, 1 h later, fluorescent lymphocytes in lymphocyte suspensions from lymphoid organs were quantified. At least four recipient mice were tested in each experiment. (**b**) For PLN, *, $P < 0.01$, versus wild-type mice; **, $P < 0.01$, versus GlcNAc6ST-1-deficient mice; ***, $P < 0.01$, versus GlcNAc6ST-2-deficient mice. For MLN, *, $P < 0.01$, versus wild-type mice; **, $P < 0.01$, versus GlcNAc6ST-1-deficient mice; ***, $P < 0.1$, versus GlcNAc6ST-2-deficient mice. (**c**) *, $P < 0.01$, versus rat IgG-injected mice. (**d**–**f**) Lymphocyte rolling assay on GlyCAM-1 from various mouse lines captured by antibody to GlyCAM-1 at concentrations of 20 μg/ml (**d**,**e**) and 50 μg/ml (**f**). Data are representative of three (**b**,**c**) or two (**d**–**f**) independent experiments.

abrogated in double-knockout mice but that L-selectin-reactive carbohydrates were still expressed in low abundance.

Lymphocyte trafficking to lymph nodes

We next determined whether lymphocyte homing was affected in double-knockout mice. The number of lymphocytes in peripheral lymph nodes was reduced by 60% in double-knockout mice compared with that in wild-type mice (**Fig. 3a**). In a short-term homing assay, mice deficient in either GlcNAc6ST-1 or GlcNAc6ST-2 had a reduction of approximately 20% or 50%, respectively, in homing of lymphocytes to peripheral lymph nodes, whereas double-knockout mice had a reduction of approximately 75% (**Fig. 3b**). The residual homing of lymphocytes to peripheral lymph nodes in double-knockout mice was apparently mediated by L-selectin, as it was reduced to background by MEL-14, an antibody blocking L-selectin function (**Fig. 3c**). Lymphocyte homing to mesenteric lymph nodes and Peyer's patches was only partially blocked by MEL-14, possibly because interactions between $\alpha_4\beta_7$ integrin and MAdCAM-1 are also involved in homing of lymphocytes to these secondary lymphoid organs[24].

The additive reduction in lymphocyte homing in the double-knockout mice was consistent with results of an *in vitro* rolling assay, in which we applied normal lymphocytes to flow chambers coated with GlyCAM-1, an HEV-specific secreted glycoprotein, from the sera of wild-type or mutant mice (**Fig. 3d–f**). We noted no lymphocyte rolling when we used lymphocytes from L-selectin-deficient mice in this assay (data not shown), indicating that the rolling was mediated exclusively by L-selectin. GlyCAM-1 derived from mutant mice deficient in either GlcNAc6ST-1 or GlcNAc6ST-2 supported less lymphocyte rolling than that from wild-type mice (**Fig. 3d**). GlyCAM-1 derived from double-knockout mice did not support lymphocyte rolling when a low density of GlyCAM-1 was used. However, there were many transiently tethered lymphocytes in the same conditions (**Fig. 3e**), suggesting that the initial tethering of lymphocytes is less affected than the rolling velocity in double-knockout mice. GlyCAM-1 derived from double-knockout mice weakly supported rolling when we used a high density of GlyCAM-1 (**Fig. 3d** versus **f**), further supporting the idea that these mice have only weak L-selectin ligand activity.

Contact hypersensitivity response

To determine the relevance of GlcNAc6ST-1 and GlcNAc6ST-2 in immune responses in pathophysiological settings, we assessed contact hypersensitivity responses in mutant mice. Double-knockout mice showed significant reductions in ear swelling and leukocyte infiltration after sensitization and challenge with the hapten DNFB (2,4-dinitrofluorobenzene; **Fig. 4a,b**). HEV-like vessels reactive with MECA-79 or

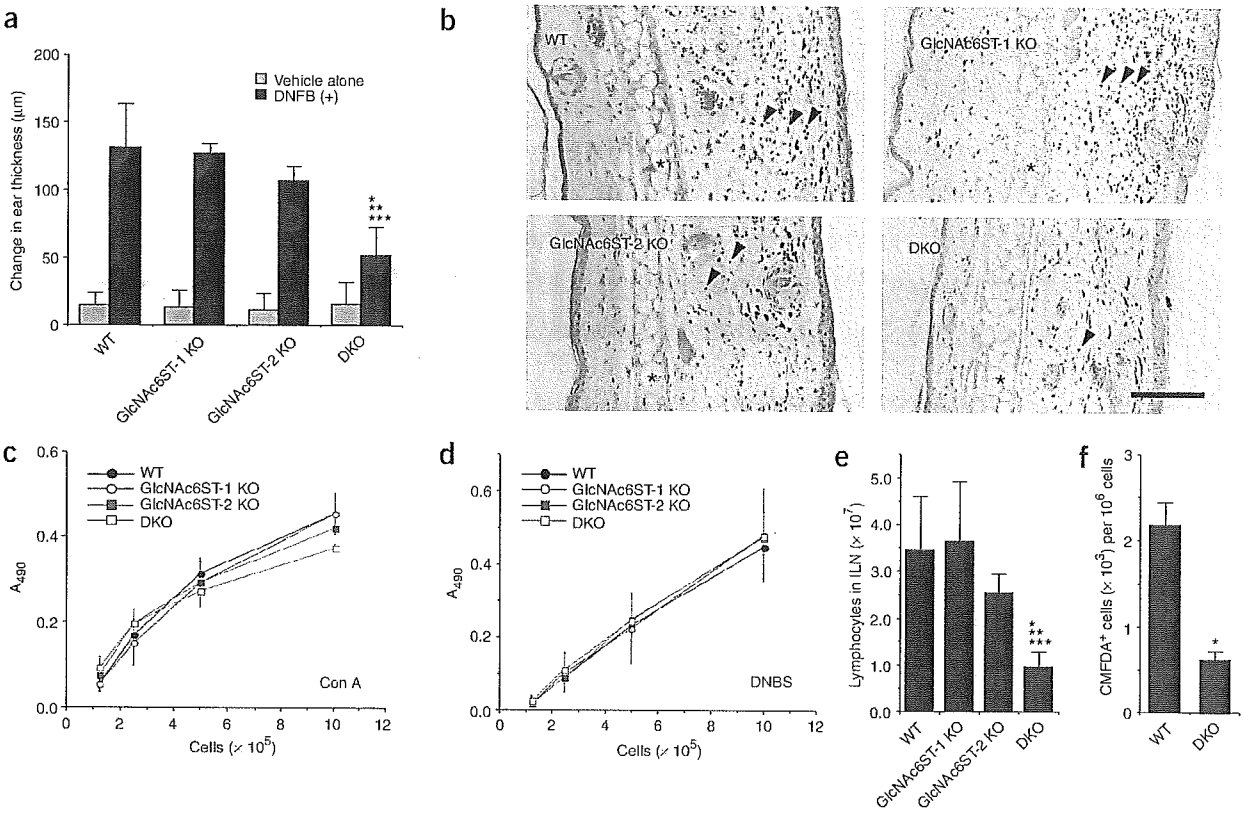

Figure 4 Reduced contact hypersensitivity in the double-knockout mice. **(a)** Ear swelling 24 h after challenge with DNFB or vehicle alone in wild-type and null mice (horizontal axis; $n = 5$). *, $P < 0.01$, versus wild-type mice; **, $P < 0.01$, versus GlcNAc6ST-1-deficient mice; ***, $P < 0.01$, versus GlcNAc6ST-2-deficient mice. **(b)** Hematoxylin-and-eosin staining of ear sections 24 h after DNFB challenge. *, ear cartilage; arrowheads, recruited leukocytes. Scale bar, 100 μm. **(c,d)** Cell proliferation assay of lymphocytes from inguinal lymph nodes sensitized with DNFB and cultured in the presence of concanavalin A (Con A; 2 μg/ml) or DNBS (200 μg/ml; $n = 3$ mice). A_{490}, absorbance at 490 nm. **(e)** Lymphocytes recovered from the inguinal lymph nodes (ILN) of DNFB-sensitized mice (horizontal axis; $n = 6$–8 mice). *, $P < 0.01$, versus wild-type mice; **, $P < 0.01$, versus GlcNAc6ST-1-deficient mice; ***, $P < 0.01$, versus GlcNAc6ST-2-deficient mice. **(f)** Trafficking of CMFDA-labeled lymphocytes to the inguinal lymph nodes of DNFB-sensitized mice (horizontal axis; $n = 3$ mice). *, $P < 0.01$, versus wild-type mice. Data (**a–d,f**) are representative of three independent experiments.

with L-sel–IgM were not detected in the ears of wild-type or mutant mice after the challenge (data not shown), suggesting that the reduction in the contact hypersensitivity response in double-knockout mice could have been due to qualitative or quantitative differences in the immune responses in the draining lymph nodes. *In vitro* proliferation of lymphocytes in response to the mitogen concanavalin A or to the water-soluble analog of DNFB, DNBS (2,4-dinitrobenzene sulfonic acid)[25], was almost indistinguishable in wild-type versus mutant mice (**Fig. 4c,d**). These data indicate that antigen-specific lymphocytes were present at almost the same ratio in the draining lymph nodes of both mouse lines. Notably, however, the total number of lymphocytes decreased by 70% in double-knockout mice (**Fig. 4e**). Consistent with that observation, lymphocyte trafficking to the draining lymph nodes significantly decreased in double-knockout mice in a short-term homing assay (**Fig. 4f**). These results collectively suggest that the reduced contact hypersensitivity response of double-knockout mice could be attributed to the quantitative decrease in the total number of antigen-specific lymphocytes recruited to the draining lymph nodes.

Carbohydrate structural analysis of GlyCAM-1

To gain insight into the structural basis of the substantial reduction in lymphocyte homing in the normal and pathophysiological conditions described above, we undertook carbohydrate structural analysis of GlyCAM-1. We first radiolabeled lymph nodes from wild-type and mutant mice with [^{3}H]galactose in organ culture and then released the *O*-glycans on GlyCAM-1 and did structural analysis. After removing sialic acid by mild acid hydrolysis, we fractionated oligosaccharides by gel filtration and anion-exchange column chromatography (**Supplementary Fig. 1** online). We then analyzed unsulfated oligosaccharides by exoglycosidase treatment and gel filtration. The amount of unsulfated oligosaccharides, including those containing the sialyl Lewis X structure, was substantially increased in double-knockout mice (**Fig. 5a**). We also analyzed sulfated oligosaccharide fractions in detail by exoglycosidase treatment and high-performance liquid chromatography (HPLC; **Supplementary Fig. 2** online). We found only very little oligosaccharide containing GlcNAc-6-*O*-sulfate in double-knockout mice (**Fig. 5a**). Conversely, the relative amount of sulfated oligosaccharides containing galactose-6-*O*-sulfate increased considerably in double-knockout mice (*O*-glycan structures, **Supplementary Fig. 3** online).

We calculated the amount of sialylated oligosaccharides from the amount of [^{3}H]galactose released by treatment of the total oligosaccharide fraction with a mixture of β-galactosidase and α-(1,3)- and α-(1,4)-fucosidase before and after the removal of sialic acid